To the Graduate Council:

I am submitting herewith a dissertation written by Joseph E. Durham entitled "Modeling Two-Point Spatial Turbulence Spectra For Analysis of Gust Variations Over Aerospace Vehicles". I have examined the final copy of this dissertation for form and content and recommend that it be accepted in partial fulfillment of the requirements for the degree of Doctor of Philosophy, with a major in Engineering Science.

Walter Frost

Walter Frost, Major Professor

We have read this dissertation and recommend its acceptance:

Ralph Kimberlin

Robert E. Turner

K R Kimble

Frank G. Collins

Bruce W. Bomar

Accepted for the Council:

C W Minkel

Vice Provost and Dean
of the Graduate School

MODELING TWO-POINT SPATIAL TURBULENCE SPECTRA FOR ANALYSIS OF GUST VARIATIONS OVER AEROSPACE VEHICLES

A Dissertation

Presented for the

Doctor of Philosophy

Degree

The University of Tennessee, Knoxville

Joseph E. Durham, Jr.

August 1990

ACKNOWLEDGEMENTS

The author wishes to express his sincere gratitude to all who have assisted him and offered encouragement during this investigation. In particular, the author gratefully acknowledges his dissertation advisor, Professor Walter Frost, who gave generously of his time, expertise, and guidance during the author's entire doctoral study program and especially during the investigation to support this dissertation.

The author also wishes to acknowledge his doctoral committee, Dr. Bruce Bomar, Dr. Frank Collins, Dr. Ralph Kimberlin, Dr. Kenneth R. Kimble, and Dr. Robert E. Turner for their professional guidance, academic instructions, and genuine interest in this research.

The author wishes to thank Mrs. Martha Craddock for typing this dissertation and Mr. Robert Suttles for preparing the final figures.

Sincere appreciation is also given to the U.S. Army Missile and Space Intelligence Center's Director, Dr. Robert G. Priddy, for his support and cooperation during the work on this dissertation. The author sincerely appreciates the valuable suggestions and helpful discussions provided by Dr. Thomas E. Richardson, Dr. Chris Ashby, and especially Dr. Mervin C. Budge.

ABSTRACT

Analytical models for two-point spatial spectra of atmospheric turbulence are developed. Models based on both the von Karman and Dryden correlation are presented. A two-point auto-correlation, defined as the correlation between like components of velocity measured at two spatially separated positions, is Fourier transformed to give the spectrum.

The bias and aliasing errors associated with fast Fourier transform techniques for two-point spatial correlations are described. A comparison is given of the spectrum computed by the fast Fourier transform of the digitized analytical correlation, with closed form solutions. The results demonstrate that the two-point spatial spectrum is extremely sensitive to bias errors. Filters for smoothing the data to minimize the bias error are investigated and an optimum filter is proposed.

TABLE OF CONTENTS

LIST OF FIGURES

FIGURE | TITLE | PAGE

LIST OF TABLES

CHAPTER I

INTRODUCTION

The effects that atmospheric turbulence has on an aircraft during landing or takeoff has a strong influence on both the structural design of the aircraft as well as the design of its aerodynamic controls. A significant amount of theoretical analysis has been devoted to computing the aerodynamic forces and the resulting pitching and rolling moments using linearized turbulence models (Diederich and Drischler (1957), Houbolt and Sen (1972), Houbolt (1973), Frost and Lin (1983), Ringnes and Frost (1985), and Frost, et al (1987)). The atmospheric turbulence used for most of the aerodynamic analysis can be grouped into two models. These two models are depicted in Figure 1. The first model assumes a linearly uniform but one-dimensional random time varying turbulence in which the turbulence is modeled as essentially rolling waves acting uniformly over the aircraft. The second model introduces two- or three-dimensional random gusts which are modeled as sinusoidally distributed in three-dimensional space. The first model introduces only pitching moments to the aircraft. The three-dimensional gust model allows both pitching and rolling moment analysis of the aircraft, as well as structural wing bending, etc. Dynamic analyses of turbulence effects on aircraft often employ models of turbulence spectra. Although many one-dimensional models are available, notable among these are the von Karman and the Dryden models, two-point spectra models which account for spatial variation in turbulence are much less available.

Houbolt and Sen (1972) developed theoretical models of two-point spatial spectra based on von Karman's correlation model. Their vertical velocity spectrum is correct but their longitudinal velocity spectrum is incorrect since they did not account for the direction cosines which align the velocity components with the body

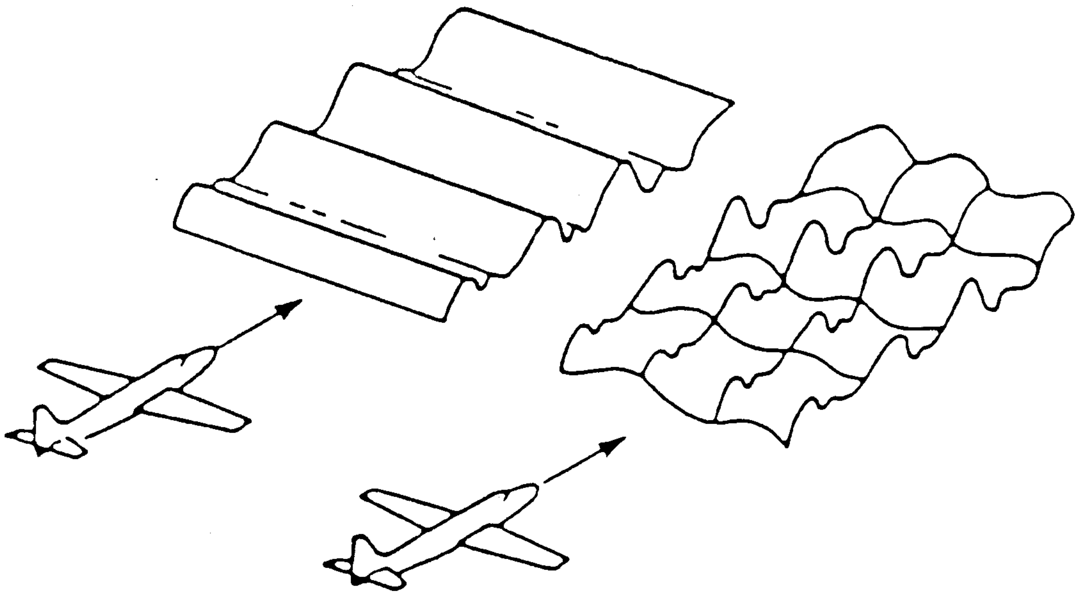

a. Assumption of Turbulence Models

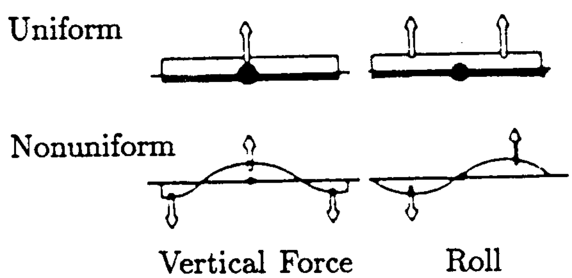

b. Random Gusts Assumed to be Composed of Sinusoidal Gusts Acting Over the Aircraft Produce Bending and Rolling Forces

Figure 1. Structure of Turbulence.

axis of the aircraft. Frost, et al. (1987) developed a correct theoretical model based on von Karman's correlation but did not fully investigate all the ramifications of their results. Moreover, no one has published a complete theoretical model of the two-point spatial spectra based on the less precise for atmospheric turbulence, but more popular due to mathematical simplicity, Dryden correlation.

As part of this research, the closed form solution for the two-point spatial spectra based on the Dryden correlation is developed. In addition, a full derivation and parametric investigation of the two-point spatial spectra based on the von Karman correlation is presented. For this analysis, the definition of "two-point" spatial correlation used by Frost, et al. (1987) was adopted. That is, the commonly used "cross-correlation" term will be used to describe a correlation between different velocity components such as lateral and longitudinal components or between vertical and lateral components. The term "two-point" spatial correlation is used to describe a correlation between velocity components measured at stations separated in space such as the two wing tips of an aircraft. There can be a "two-point" cross-correlation between different velocity components separated spatially or a "two-point" correlation between like velocity components separated spatially. The term auto-correlation is used to define a correlation between like velocity components measured at the same spatial location but separated in time.

The current practice used by the atmospheric community to compute turbulent spectra is direct Fourier transform of the measured digitized velocity fluctuation time history. This is referred to as a direct Fourier transform. The alternate approach is to first compute the correlation and then Fourier transform it to obtain the spectra. In both cases the data are digitized and a Discrete Fourier Transform (DFT) technique is employed. The Fourier transform of a digitized signal, however, can introduce both bias and aliasing errors. A systematic study of the nature of these errors in atmospheric turbulence analyses has not been reported in the literature. Therefore, a second part of this research is to investigate these errors in a systematic fashion. Having developed in the first part a closed form solution for the spectra by direct integration of the theoretical correlation, an analysis of the effects of using DFT to integrate the correlation in a digitized format can be conducted. The analysis investigates the effects of record lengths which introduce bias errors and the effects of sampling intervals (digitizing time step) which introduce aliasing errors. Recommendations for using DFT analysis on measured data sets is presented. In addition, an investigation of using windowing techniques to resolve bias errors is included. This results in the recommendation of one or more selected windowing techniques which should be applied in atmospheric turbulence spectral analysis.

CHAPTER II

ANALYTICAL MODEL OF THE TWO-POINT SPATIAL SPECTRA FOR ATMOSPHERIC TURBULENCE

A two-point spatial spectrum may be computed by a Fourier transform of the correlation for atmospheric turbulence. In this chapter the classical (along the x_1 axis in ground fixed coordinates) longitudinal and lateral (along the x_2 or x_3 axis in ground fixed coordinates) correlations for turbulence are extended to correlations in a general coordinate system which is aligned with the body axis of an aircraft. The extended correlations are then analytically integrated to produce closed form solutions of the spectra for direction 1 (along body), direction 2 (along wing span), and direction 3 (along perpendicular to plane of wing and body) velocity components in the aircraft body axis coordinate system. A graphical presentation of the solutions for a range of parameters is then given at the end of this chapter.

The general turbulence correlation tensor can be developed following the work of Hinze (1975). Consider two points A and B in a flow field with $\vec{a}$ and $\vec{b}$ being two given directions at each of the points A and B, Figure 2. If the mean velocity of the flow field is assumed to be constant, then at any instant

$$\begin{aligned} U_a &= U_1 e_{a1} + u_a \\ U_b &= U_1 e_{b1} + u_b \end{aligned} \tag{1}$$

where the direction cosines of the flow with respect to the mean flow are e_{a1} and e_{b1}. The velocities U_a and U_b consist of a mean velocity and a turbulent fluctuation about the mean. The correlation of velocities U_a and U_b is given as

$$\begin{aligned} \overline{U_a(\vec{x}_A)\, U_b(\vec{x}_B)} &= \overline{(U_1 e_{a1} + u_a)_A\, (U_1 e_{b1} + u_b)_B} \\ &= U_1^2 e_{a1} e_{b1} + \overline{(u_a)_A\, (u_b)_B} \end{aligned} \tag{2}$$

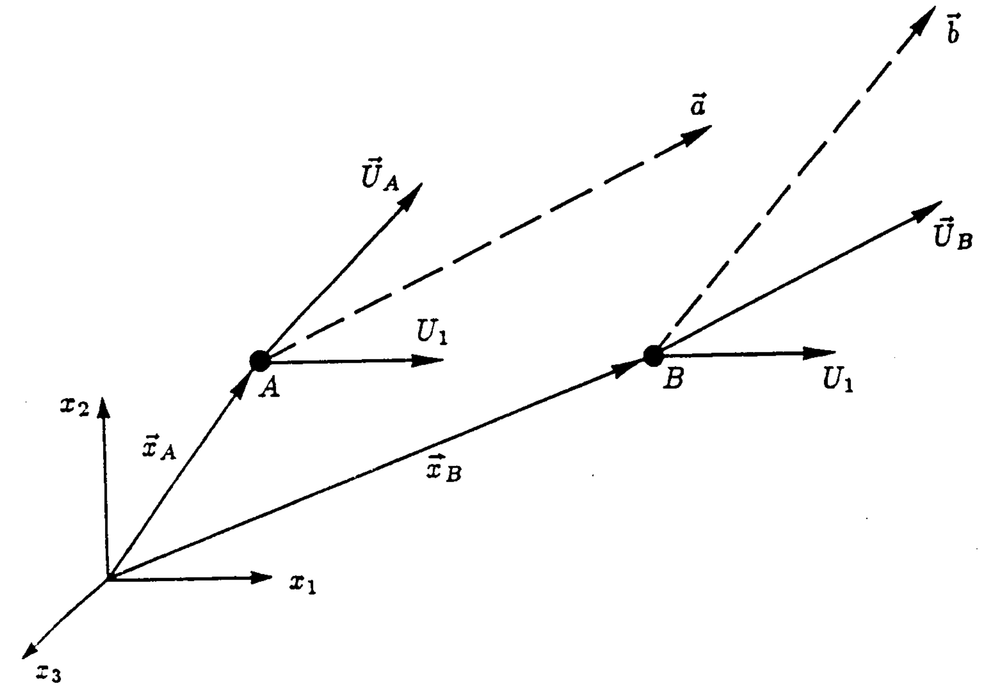

Figure 2. Notations for Definition of General Flow Field Turbulence Correlation Tensor.

where the first term on the right-hand side of Equation 2 relates to the mean motion of the flow field and the second term relates to the turbulent fluctuations in the flow field. Since the mean flow pattern does not vary with time in a steady flow field, the correlation product given in Equation 2 is a function of the location of points A and B and the turbulent components u_a and u_b at those points, i.e.:

$$Q_{A,B} = \overline{(u_a)_A \ (u_b)_B} \tag{3}$$

If the turbulent velocities are defined in terms of the velocity components $(u_i)_A$ and $(u_i)_B$ along a selected Cartesian coordinate axis, such that

$$Q_{A,B} = \overline{(u_i)_A \ (u_j)_B} \ e_{ai}e_{bi} \tag{4}$$

then the term $\overline{(u_i)_A \ (u_j)_B}$ becomes a tensor of second-order

$$(Q_{i,j})_{A,B} = \overline{(u_i)_A \ (u_j)_B} \tag{5}$$

Defining ξ_k as the Eulerian cartesian coordinates relating the position of A to B, then it can be shown that $Q_{A,B}$ is a function of ξ_k, e_{aj} and e_{bj} given by

$$Q_{A,B} = Q_1\xi_i\xi_j e_{ai}e_{aj} + Q_2\delta_{ij}e_{ai}e_{aj} + Q_3\epsilon_{ijk}\xi_k e_{ai}e_{bj} \tag{6}$$

where δ_{ij} is a unit second-order tensor (Kronecker Delta), ξ_{ijk} is an alternating unit tensor and Q_1, Q_2, and Q_3 are functions of r^2 where r is the distance between points A and B. The correlation component $(Q_{i,j})_{A,B}$ becomes

$$(Q_{i,j})_{A,B} = Q_1\xi_i\xi_j + Q_2\delta_{ij} + Q_3\epsilon_{ijk}\xi_k \tag{7}$$

The remainder of the derivation assumes the flow field is both homogeneous and isotropic. These conditions require that for an arbitrary point there can be no variance of the correlation under rotation of the coordinate system and under reflection with respect to the coordinate system, therefore

$$(Q_{i,j})_{A,B} = (Q_{j,i})_{A,B} \tag{8}$$

which requires $Q_3 = 0$. Equation 7 then becomes

$$(Q_{i,j})_{A,B} = Q_1(r^2)\xi_i\xi_j + Q_2(r^2)\delta_{ij} \tag{9}$$

Equation 9 is the general expression for a homogeneous, isotropic tensor of the second order.

Defining the term $f(r)$ as the coefficient of spatial longitudinal velocity correlation with respect to r and the term $g(r)$ as the corresponding lateral velocity correlation, Figure 3, Equation 9 can be written as

$$(Q_{i,j})_{A,B} = u'^2 \left[\frac{f(r) - g(r)}{r^2} \, \xi_i\xi_j + g(r)\delta_{ij} \right] \tag{10}$$

where u' is defined as $\sqrt{\overline{u^2}}$ which is the root-mean-square of the turbulent velocity component.

Consider now an aircraft flying in a horizontal plane with a constant mean velocity, V. Point A is on the left wing tip and Point B is a point upstream of the right wing tip. This point will, in principle, impinge upon the wing at a later time, t, as shown in Figure 4. Thus, as the aircraft flies through a non-aligned atmospheric flow field with a velocity, V, the gust experienced at the right wing tip which occurs at a lag time, t from that experienced by Point A, is itself at point B. Assuming Taylor's hypothesis (Taylor (1938)), turbulence at B is an effective distance, r, from A given by

$$r = \sqrt{s^2 + V^2t^2}$$

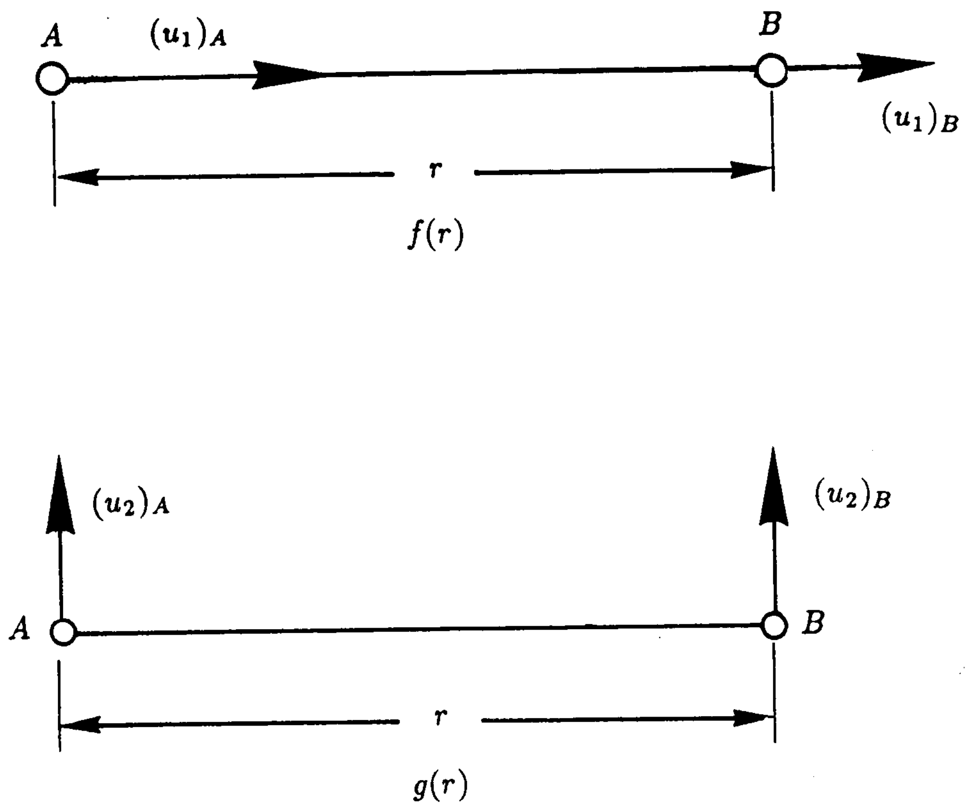

$$f(r) = (Q_{1,1})_{A,B} \; / \; u'^2 = \overline{(u_1)_A (u_1)_B} \; / \; u'^2$$

$$g(r) = (Q_{2,2})_{A,B} \; / \; u'^2 = (Q_{3,3})_{A,B} \; / \; u'^2 = \overline{(u_2)_A (u_2)_B} \; / \; u'^2$$

$$u'^2 = \overline{u_i u_i}, \quad i = 1,\ 2,\ \text{or } 3$$

Figure 3. Definition of the Longitudinal and Lateral Velocity Correlations, $f(r)$ and $g(r)$.

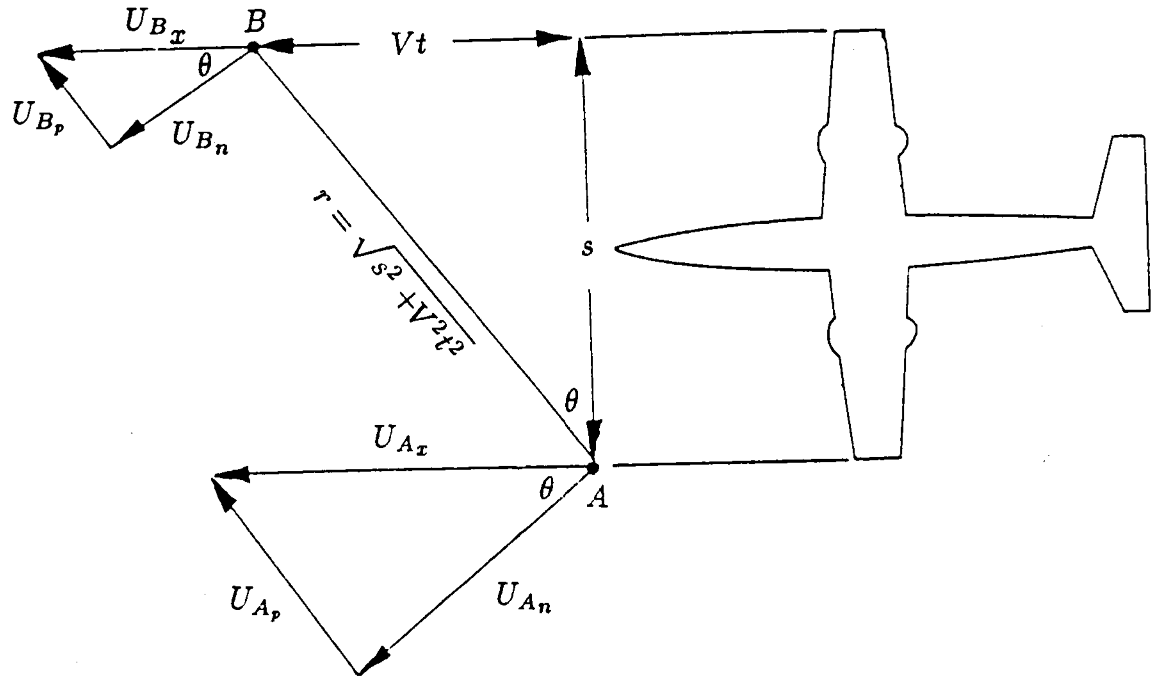

Figure 4. Aircraft Velocity Components.

Moreover, the sine and cosine of the angle θ are given by

$$sin\theta = Vt \;/\; \sqrt{s^2 + V^2t^2}$$
$$cos\theta = s \;/\; \sqrt{s^2 + V^2t^2} \tag{11}$$

In terms of these definitions, the correlations for the velocity component given by Equation 10 becomes

$$(Q_{1,1})_{A,B} = u_1'^2 \left[\frac{f(r) - g(r)}{r^2}\,(Vt)^2 + g(r) \right]$$
$$(Q_{2,2})_{A,B} = u_2'^2 \left[\frac{f(r) - g(r)}{r^2}\,(s)^2 + g(r) \right] \tag{12}$$
$$(Q_{3,3})_{A,B} = u_3'^2 \left[g(r) \right]$$

The two-point spatial spectra $(E_{i,j})_{A,B}$ is defined as the Fourier transform of the correlation $(Q_{i,j})_{A,B}$

$$(E_{i,j})_{A,B} = \int_{-\infty}^{\infty} (Q_{i,j})_{A,B}\; e^{-i\omega t}\; dt \tag{13}$$

Equation 13 can be evaluated upon substituting $(Q_{i,j})$ in the form of Equation 12 after appropriate selection of the functional form of $f(r)$ and $g(r)$.

Von Karman (1948) developed theoretical expressions for $f(r)$ and $g(r)$ which have been found to fit atmospheric data well. The von Karman correlations are functions of the modified Bessel function of the second kind, $K_p(\;)$, as defined in Lebedev (1972), and are given by

$$f(r) = \frac{2^{2/3}}{\Gamma(1/3)} \left(\frac{r}{L}\right)^{1/3} K_{1/3}\left(\frac{r}{L}\right)$$

and

$$g(r) = \frac{2^{2/3}}{\Gamma(1/3)} \left(\frac{r}{L}\right)^{1/3} \left[K_{1/3}\left(\frac{r}{L}\right) - \frac{r}{2L}\, K_{2/3}\left(\frac{r}{L}\right) \right] \tag{14}$$

where $\Gamma(\ )$ is the Gamma function and L is a length scale characterizing the eddy sizes of the turbulence. Substituting Equations 14 into Equations 12 gives the von Karman correlations in the aircraft body coordinates as

$$
\begin{aligned}
Q_{11}(l) &= H_1\left[\ell^{1/3}\, K_{1/3}(\ell) - \left(\frac{1}{2}\right)\left(\frac{\sigma}{a}\right)^2 \ell^{-2/3}\, K_{2/3}(\ell)\right] \\
Q_{22}(l) &= H_2\left[\left(\frac{4}{3}\right)\ell^{1/3}\, K_{1/3}(\ell) + \left(\frac{1}{2}\right)\left(\frac{\sigma}{a}\right)^2 \ell^{-2/3}\, K_{-2/3}(\ell)\right. \\
&\qquad \left. - \left(\frac{1}{2}\right)\ell^{4/3}\, K_{4/3}(\ell)\right] \\
Q_{33}(l) &= H_3\left[\left(\frac{4}{3}\right)\ell^{1/3}\, K_{1/3}(\ell) - \left(\frac{1}{2}\right)\ell^{4/3}\, K_{4/3}(\ell)\right]
\end{aligned}
\tag{15}
$$

where the nomenclature for Q and E is changed slightly, from this point on, for convenience of presentation.

$$
\begin{aligned}
H_i &= u_i'^2\ 2^{2/3} \ /\ \Gamma(1/3) \\
l &= \frac{\sqrt{s^2 + V^2t^2}}{aL} \ ; \ \sigma = s/L \\
a &= \sqrt{\pi}\ \Gamma(1/3)\ /\ \Gamma(5/6) = 1.339
\end{aligned}
$$

as defined in von Karman (1948).

Applying the Fourier transform, Equation 13, to these correlations results in the two-point spatial spectra

$$
\begin{aligned}
E_{11}(\nu) &= Cu_1'^2\sigma^{5/3}\left\{K_{-5/6}[z]z^{-5/6} - \frac{1}{2}\, K_{1/6}[z]z^{1/6}\right\} \\
E_{22}(\nu) &= Cu_2'^2\sigma^{5/3}\left\{\frac{4}{3}\, K_{-5/6}[z]z^{-5/6} + \frac{1}{2}\, K_{1/6}[z]z^{1/6} - \frac{1}{2}\,\frac{\sigma^2}{a^2}\, K_{-11/6}[z]z^{-11/6}\right\} \\
E_{33}(\nu) &= Cu_3'^2\sigma^{5/3}\left\{\frac{4}{3}\, K_{-5/6}[z]z^{-5/6} - \frac{1}{2}\,\frac{\sigma^2}{a^2}\, K_{-11/6}[z]z^{-11/6}\right\}
\end{aligned}
\tag{16}
$$

where

$$z = \sigma\left\{\nu^2 + (1/a)^2\right\}^{1/2}$$

$$\nu = \omega L/V; \quad \sigma = s/L$$

$$C = 2^{2/3}(2\pi)^{1/2} \ / \ (\Gamma(1/3) \ a^{2/3}$$

The functions $Q_{ii}(l)$ and $E_{ii}(\nu)$ become dimensionless when divided by $u_i'^2$. Thus, $Q_{ii}(l) \ / \ u_i'^2$ and $E_{ii}(\nu) \ / \ u_i'^2$ are both functions of the dimensionless parameter $\sigma = s/L$ and individually functions of the dimensionless variables $l = t \ V/L$ and $\nu = \omega \ L/V$, respectively. However, to better illustrate the influence of V/L, the plots presented in this dissertation are in dimensional form. A complete derivation of Equations 15 and 16 is given in Appendix A.

Figure 5a is a plot of the correlations for velocity components in direction 3 from Equation 15 as a function of point separation, s, divided by length scale, L. Figure 5b is the corresponding spectra. Results are presented for a fixed ratio of length scale, L, to velocity, V, of 2.0. Figure 6, on the other hand, presents the effects of holding s/L fixed at 0.10 and varying L/V from 1.0 to 5.0; all other conditions being the same.

Prior to von Karman, Dryden (1943) published the correlation for turbulence as an exponentially decaying function

$$f(r) = e^{-r/L}$$

$$g(r) = \left(1 - \frac{r}{2L}\right) e^{-r/L} \tag{17}$$

This correlation does not fit atmospheric turbulence as well as von Karman's correlation (Equation 14). However, it does agree with wind tunnel data well and it is frequently used in aeronautical analysis because the corresponding one-point spectrum is a rational function and simpler to employ mathematically. For these reasons the two-point correlations and spectra based on Dryden's model are derived

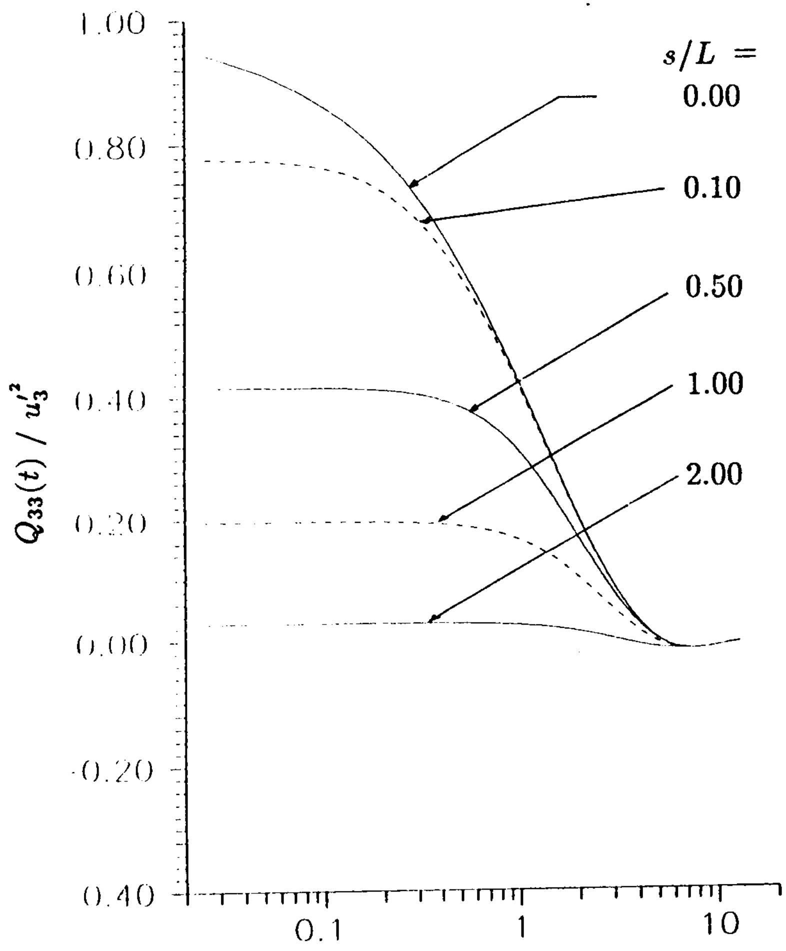

a. Correlations in Direction (3,3)

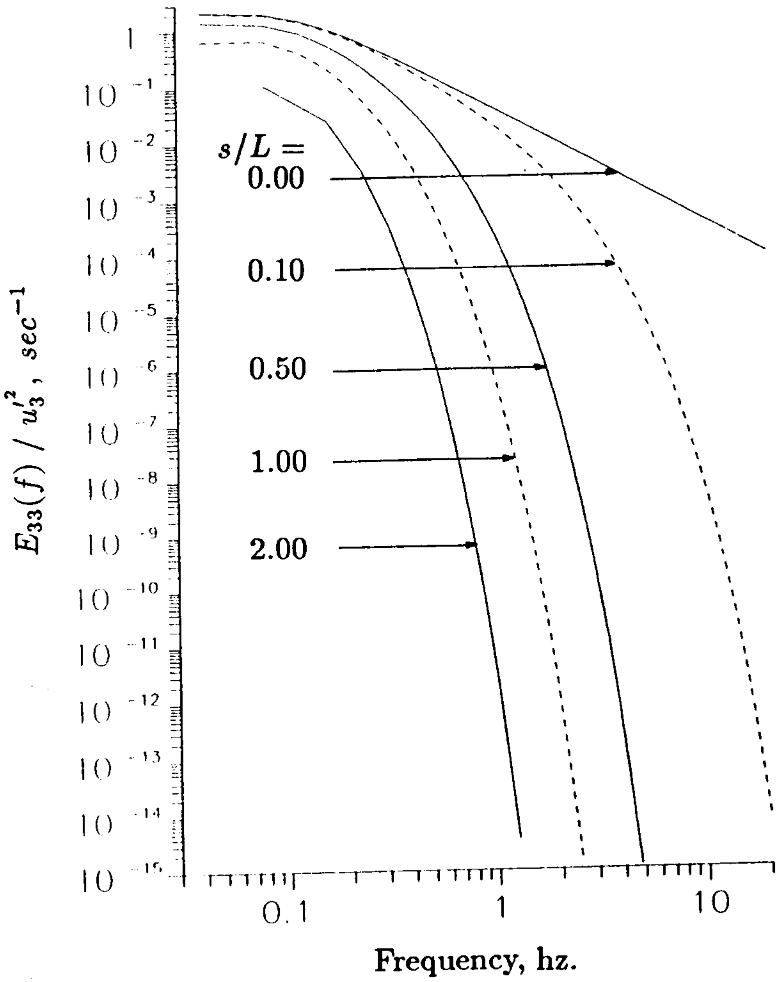

b. Spectra in Direction (3,3)

Figure 5. von Karman Correlations and Closed Form Solution Spectra, $(L/V = 2.0)$.

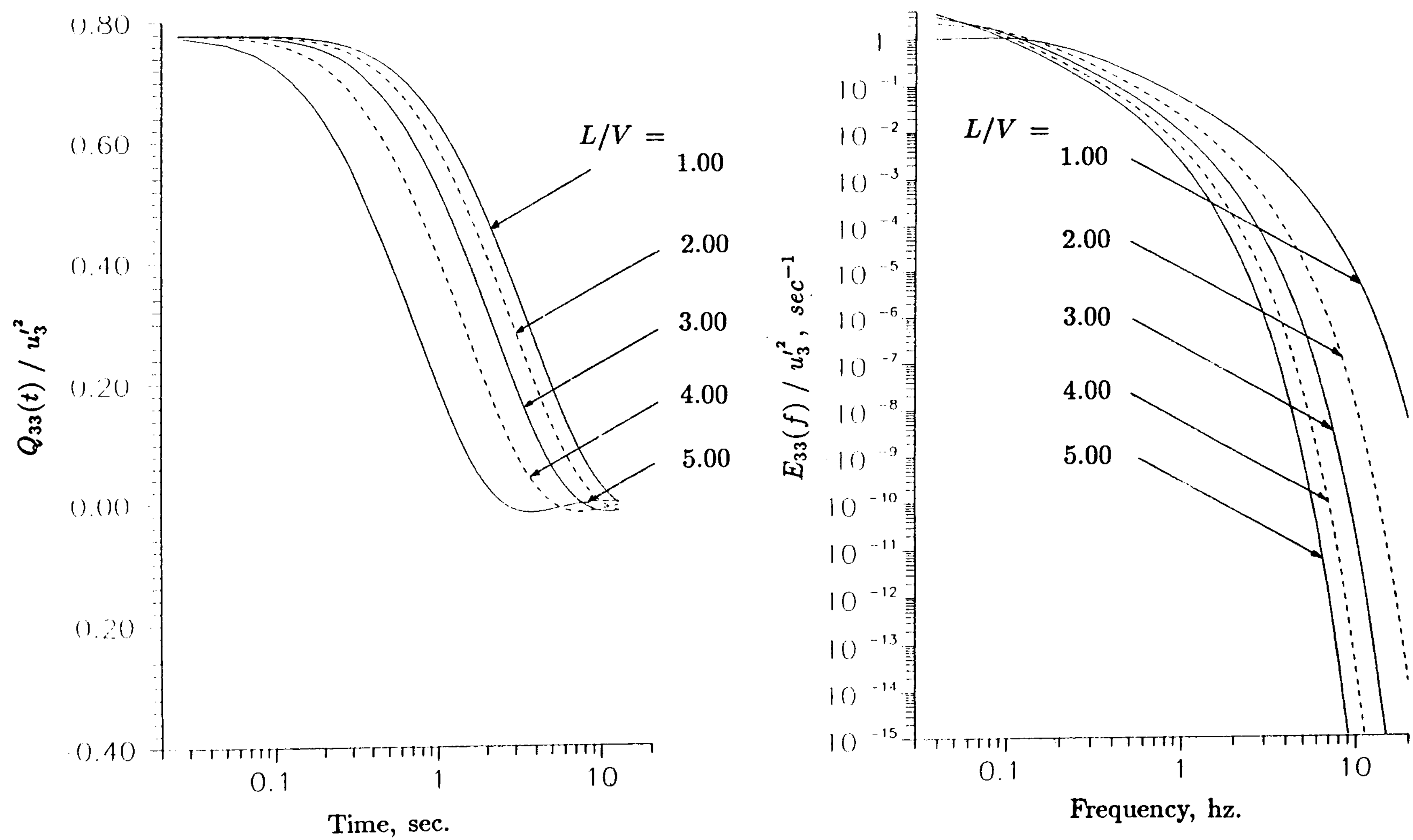

a. Correlations in Direction (3,3)

b. Spectra in Direction (3,3)

Figure 6. von Karman Correlations and Closed Form Solution Spectra, ($s/L = 0.10$).

in this study. The derivation follows the same procedure as that for the von Karman and is described in detail in Appendix B.

The two-point Dryden correlations are given by Equation 18.

$$Q_{11}(l) = u_1'^2 \left[e^{-\left(\frac{V}{L}\right)\left[\left(\frac{s}{V}\right)^2+t^2\right]^{\frac{1}{2}}} - \left(\frac{s^2}{2VL}\right) \frac{e^{-\left(\frac{V}{L}\right)\left[\left(\frac{s}{V}\right)^2+t^2\right]^{\frac{1}{2}}}}{\left[\left(\frac{s}{V}\right)^2+t^2\right]^{\frac{1}{2}}} \right]$$

$$Q_{22}(l) = u_2'^2 \left[e^{-\left(\frac{V}{L}\right)\left[\left(\frac{s}{V}\right)^2+t^2\right]^{\frac{1}{2}}} + \left(\frac{s^2}{2VL}\right) \frac{e^{-\left(\frac{V}{L}\right)\left[\left(\frac{s}{V}\right)^2+t^2\right]^{\frac{1}{2}}}}{\left[\left(\frac{s}{V}\right)^2+t^2\right]^{\frac{1}{2}}} - \left(\frac{V}{2L}\right) \frac{e^{-\left(\frac{V}{L}\right)\left[\left(\frac{s}{V}\right)^2+t^2\right]^{\frac{1}{2}}}}{\left[\left(\frac{s}{V}\right)^2+t^2\right]^{-\frac{1}{2}}} \right] \tag{18}$$

$$Q_{33}(l)_{A,B} = u_3'^2 \left[e^{-\left(\frac{V}{L}\right)\left[\left(\frac{s}{V}\right)^2+t^2\right]^{\frac{1}{2}}} - \left(\frac{V}{2L}\right) \frac{e^{-\left(\frac{V}{L}\right)\left[\left(\frac{s}{V}\right)^2+t^2\right]^{\frac{1}{2}}}}{\left[\left(\frac{s}{V}\right)^2+t^2\right]^{-\frac{1}{2}}} \right]$$

The expressions in Equation 17 contain three exponential forms. Using Equation 13 to derive the Fourier transform of Equation 17 would appear from inspection to be a much simpler task than deriving the two-point spatial spectra from the von Karman correlations. This assumption, however, turned out to be in error. A review of all published Fourier transforms revealed that there was no available transform for the last term of each expression in Equation 17. Therefore, it was necessary to derive the following Fourier transform (see Appendix B).

$$\int_0^{\infty} \left[\left(\frac{s}{V}\right)^2 + t^2\right]^{\frac{1}{2}} e^{-\left(\frac{V}{L}\right)\left[\left(\frac{s}{V}\right)^2+t^2\right]^{\frac{1}{2}}} cos(\omega t)\, dt = \left(\frac{s}{V}\right)^2 K_1(z)(z)^{-1} + \left(\frac{s}{V}\right)^4 \left(\frac{V}{L}\right)^2 K_2(z)(z) \tag{19}$$

where

$$z = \sigma\left(\left(\frac{\omega L}{V}\right)^2 + 1\right)^{\frac{1}{2}}$$

The resulting closed form solution for the two-point spatial spectra from the Fourier transform of the Dryden correlations are

$$E_{11}(\nu) = 2u_1'^2 \sigma^2 \left\{ K_1[z]z^{-1} - \left(\frac{1}{2}\right) K_o[z] \right\}$$

$$E_{22}(\nu) = 2u_2'^2 \sigma^2 \left\{ \left(\frac{3}{2}\right) K_1[z]z^{-1} + \left(\frac{1}{2}\right) K_o[z] - \left(\frac{1}{2}\right) \sigma^2 K_2[z]z^{-2} \right\} \qquad (20)$$

$$E_{33}(\nu) = 2u_3'^2 \sigma^2 \left\{ \left(\frac{3}{2}\right) K_1[z]z^{-1} - \left(\frac{1}{2}\right) \sigma^2 K_2[z]z^{-2} \right\}$$

where

$$\nu = \omega L/V$$

and

$$\sigma = s/L$$

Figure 7a is a plot of the Dryden two-point correlation from Equation 17 presented as a function of s/L and $L/V = 2$, while Figure 7b presents the corresponding spatial spectra. In Figure 8 the effects of holding s/L fixed at 0.10 and varying L/V from 1.0 to 5.0 is shown.

A quick inspection of Figures 5 through 8 reveals that both the correlations and the two-point spectra from the von Karman model compares in shape with those from the Dryden model. Figure 9 presents a direct comparison between the Dryden and von Karman models for a fixed L/V of 2.0 and for three values of s/L (0.0, 0.5, and 1.0). The Dryden correlations have a larger magnitude at low frequencies and a steeper slope than the von Karman correlations causing the correlation plots to cross. For higher values of s/L, the spectra appear merged at the higher frequencies. This is an illusion from the graphics and, in fact, the error $\left[(E_{ii}(\nu))_{VK} - (E_{ii}(\nu))_{DRY}\right] / (E_{ii}(\nu))_{VK}$ becomes progressively larger for a given frequency as shown in Figure 10.

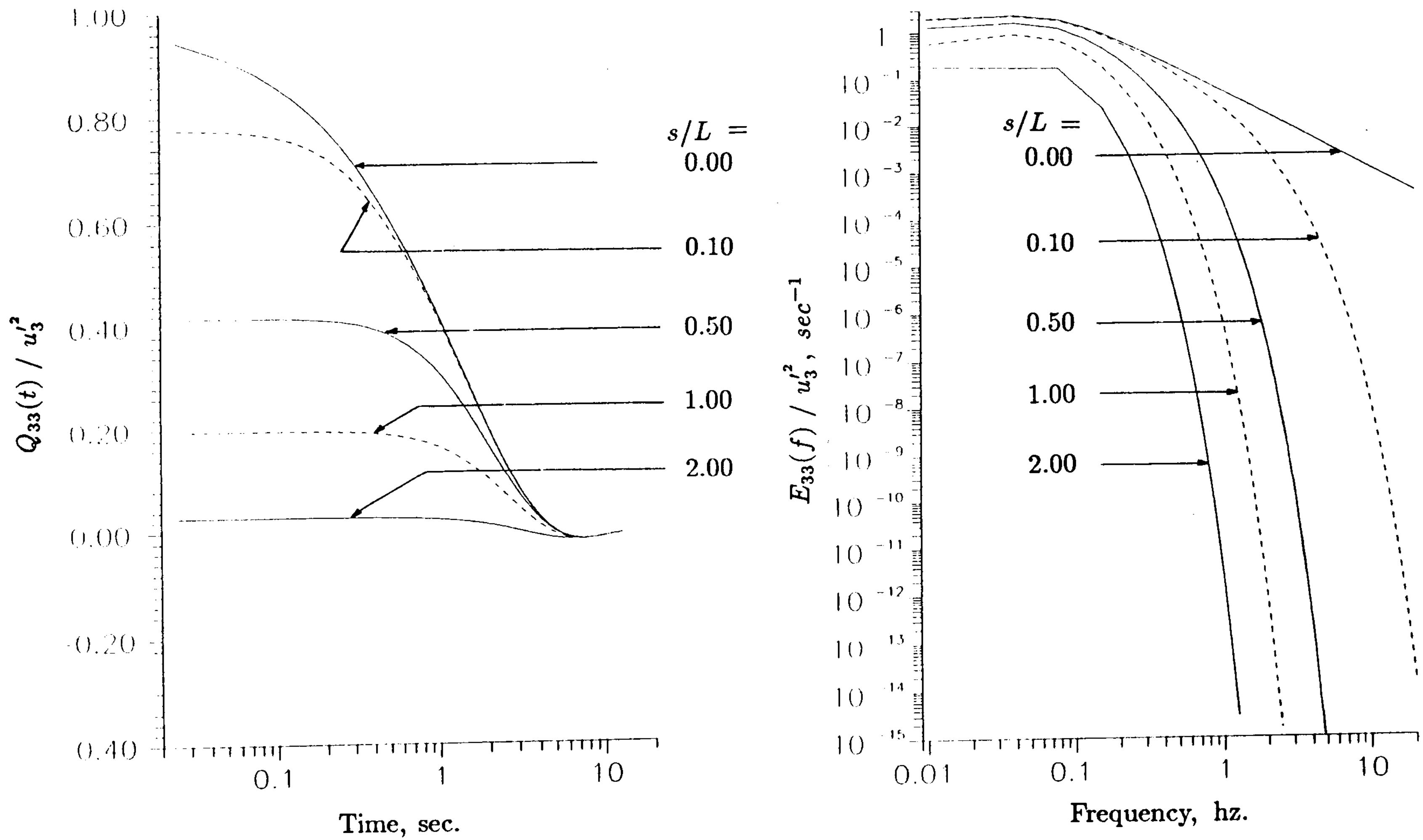

a. Correlations in Direction (3,3)

b. Spectra in Direction (3,3)

Figure 7. Dryden Correlations and Closed Form Solution Spectra, $(L/V = 2.0)$.

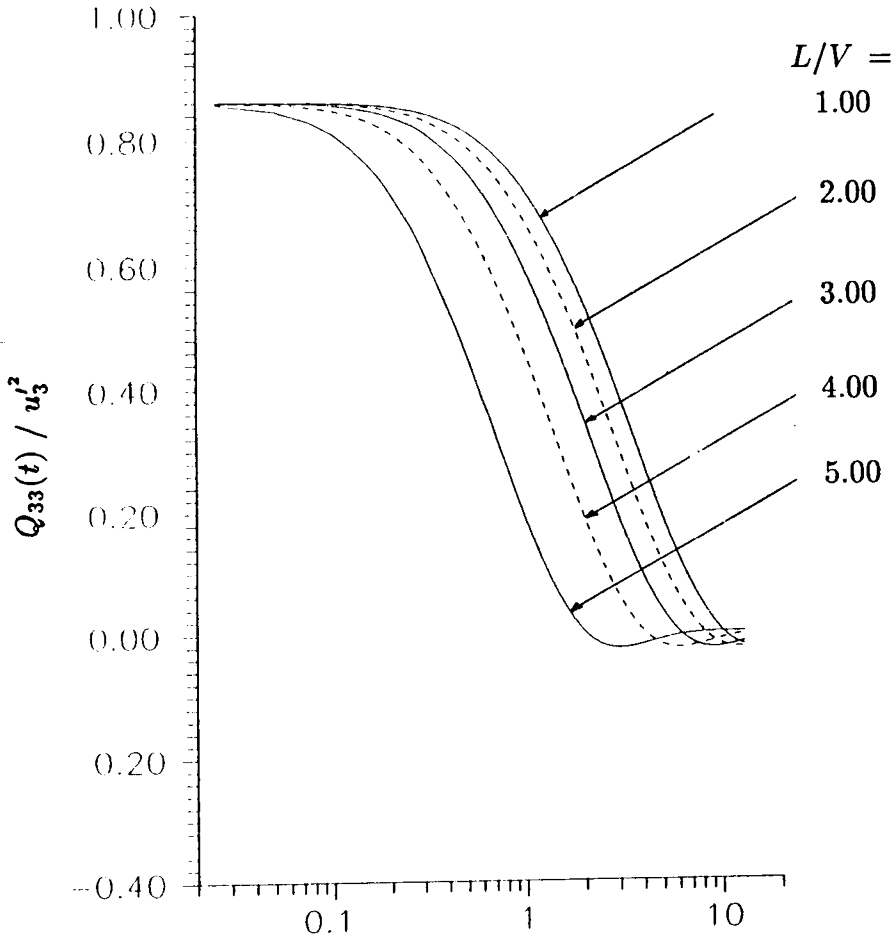

a. Correlations in Direction (3,3)

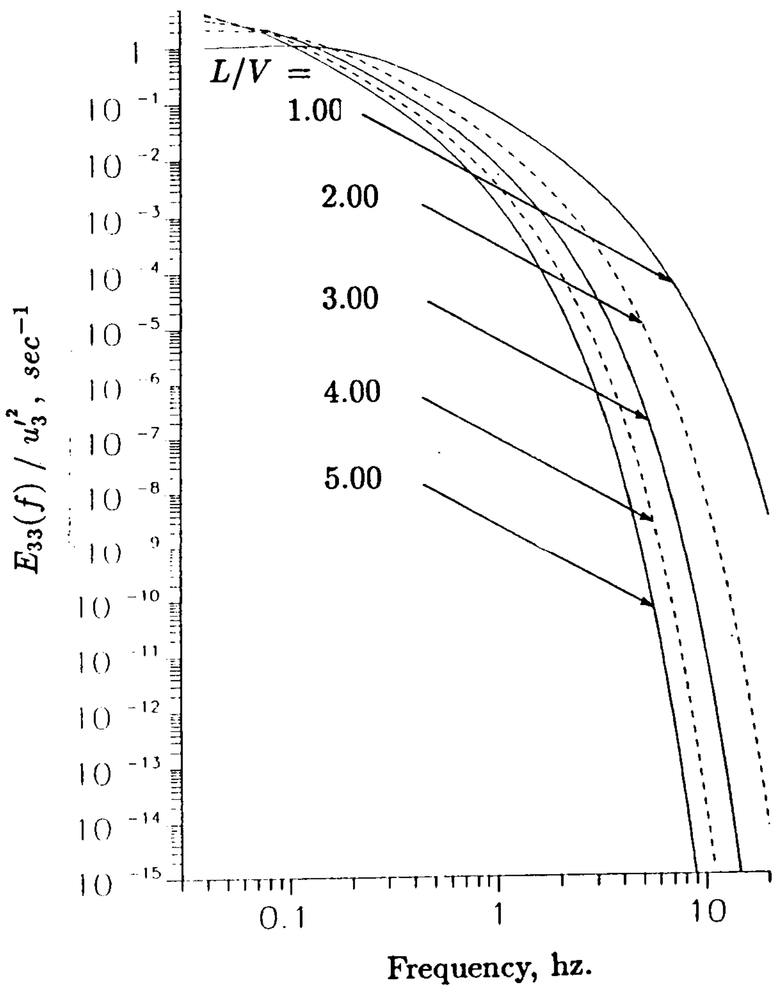

b. Spectra in Direction (3,3)

Figure 8. Dryden Correlations and Closed Form Solution Spectra, ($s/L = 0.10$).

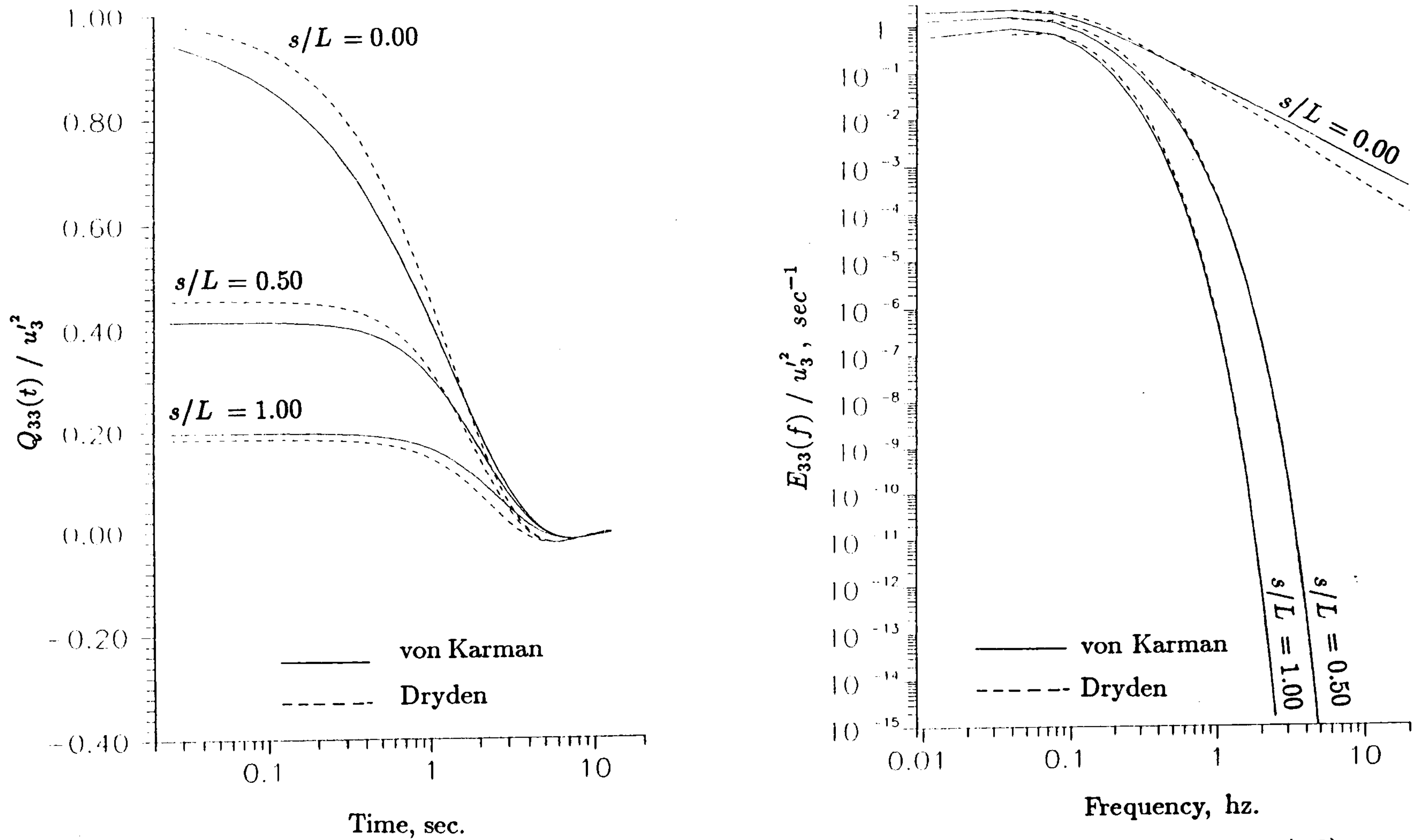

a. Correlations in Direction (3,3)

b. Spectra in Direction (3,3)

Figure 9. Comparison of von Karman and Dryden Correlations and Closed Form Solution Spectra ($L/V = 2.0$).

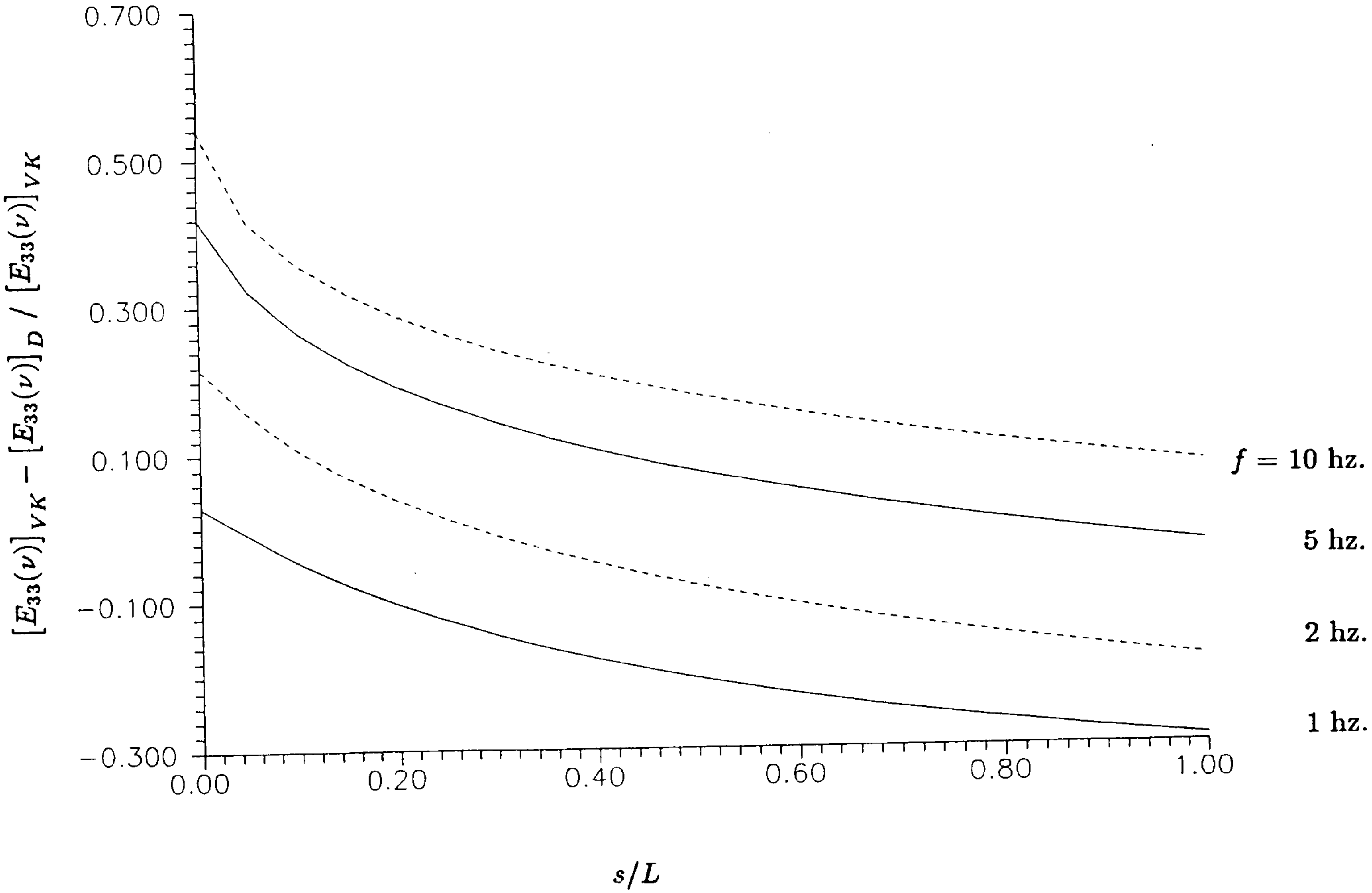

Figure 10. Percent Difference in von Karman and Dryden Spectra as a Function of s/L.

One also observes from Figure 9 that there is a faster drop-off in the lateral correlations than the longitudinal correlation which was confirmed by experimental data collected and analyzed by Kader, et al. (1989). Dryden developed his correlation model based on wind tunnel data where as von Karman developed his correlations based on atmospheric data.

It should be noted that the spectra models given in Equation 16 for von Karman and Equation 20 for Dryden are both functions of modified Bessel functions of the second kind. The Bessel functions of fractional order in the von Karman model are much more difficult to compute than the integer order Bessel functions in the Dryden model. For this study both the fractional and integer order Bessel functions were computed using an International Standard Mathematical Library (ISML) routine for personel computers. The ISML routine has a quoted accuracy of 8 to 10 digits for all modified Bessel functions and can be double precisioned. In a side-by-side comparison on a Compaq 386-20 MHz computer using a math co-processor, the computation of a given Dryden spectra was 3.5 times faster than the computation of the same von Karman spectra. On an IBM-XT 4 MHz computer, also using a math co-processor, the Dryden computation was again over 3.5 times faster.

If the ISML routine is not available, an engineer can hand compute selected points by using the Dryden model since the integer order Bessel functions, K_0 and K_1, are published in tabular form in Abramowitz and Stegun (1964). It will also be necessary to use the recursive relationship given by Lebedev (1972) which expresses K_2 as a function of K_0 and K_1 to compute all of the terms in Equation 20.

Figures 11 and 12 present the von Karman and Dryden correlations and corresponding spectra for values of $s/L = 0.2$ and $L/V = 4.0$ for each of the three directional components, respectively. The lobe shown in both spectra plots for velocity Component 1 is due to the fact that both the von Karman and Dryden models

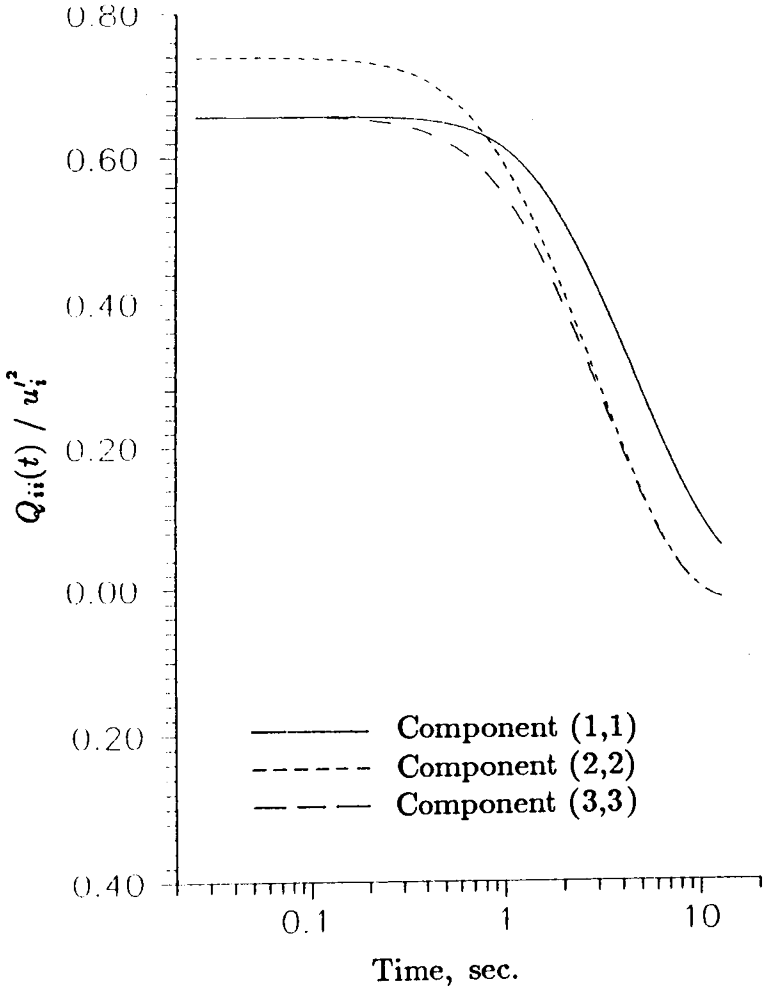

a. Correlations in Direction (1,1), (2,2), and (3,3)

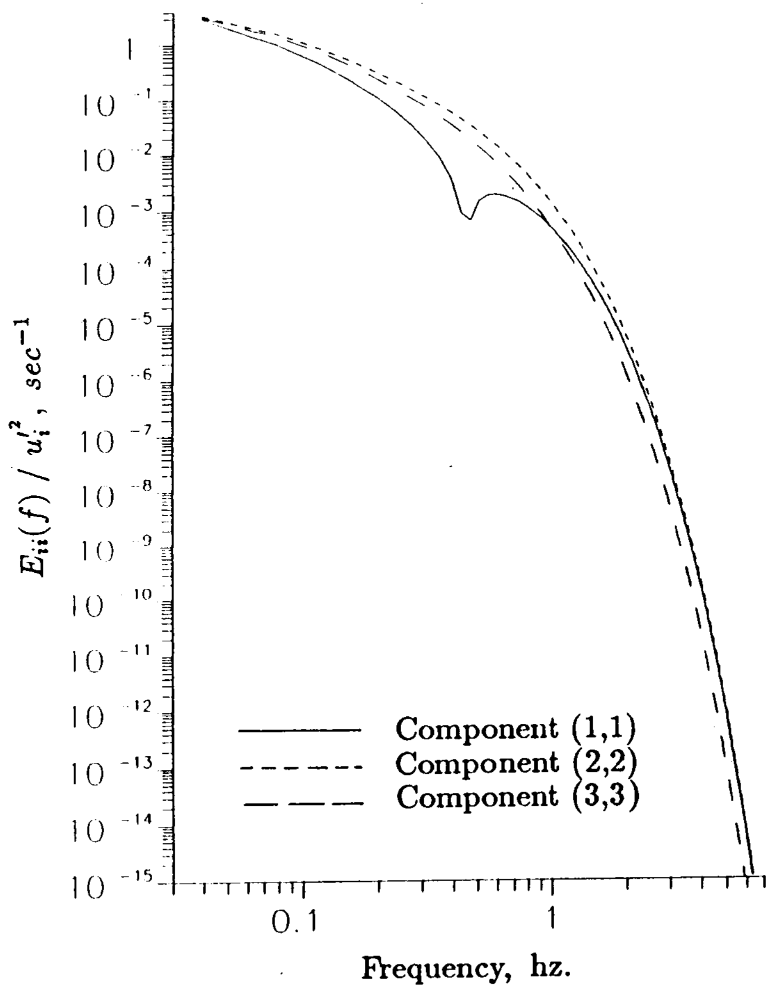

b. Spectra in Direction (1,1), (2,2), and (3,3)

Figure 11. von Karman Correlations and Closed Form Solution Spectra, ($L/V = 4.0$; $s/L = 0.20$).

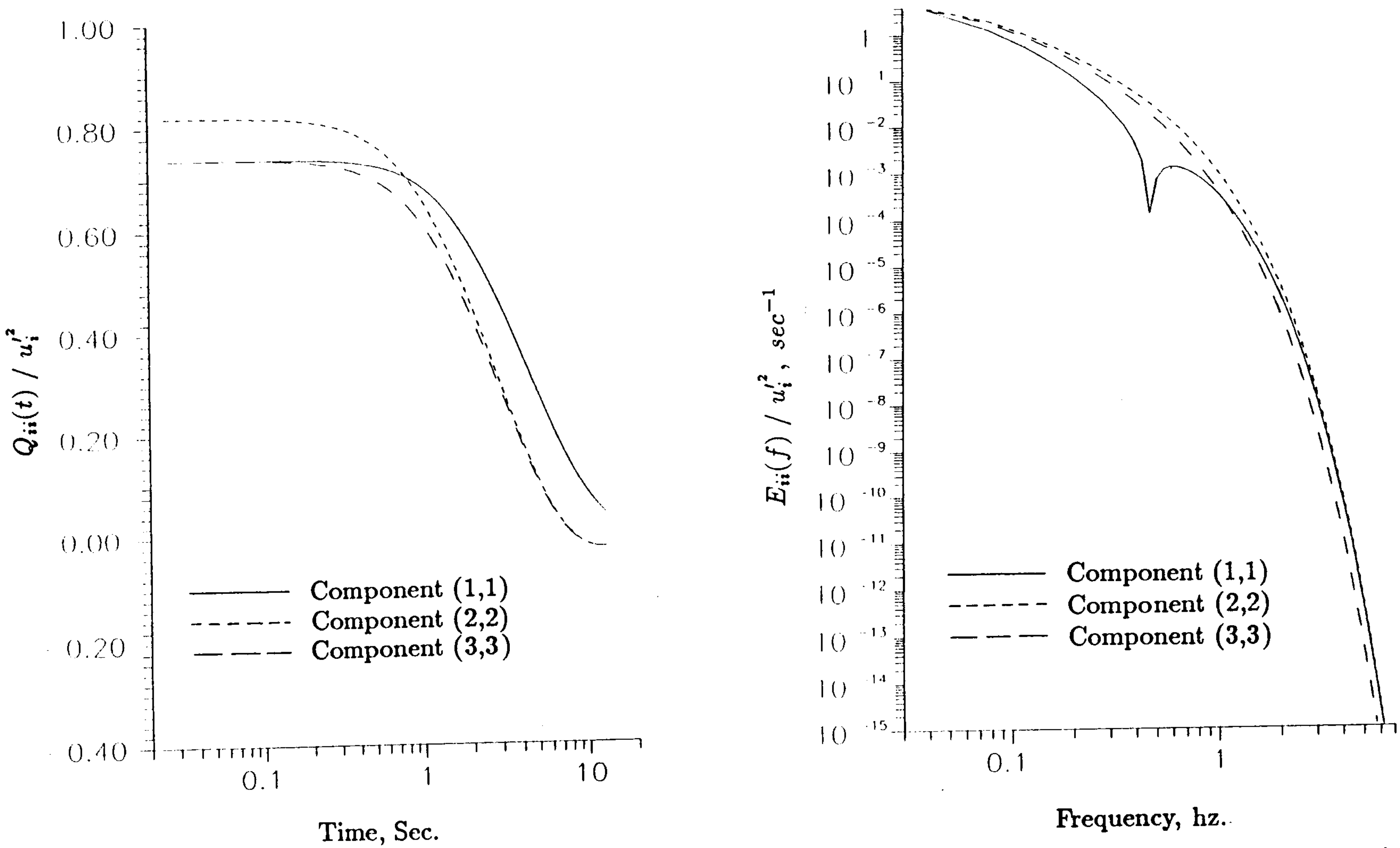

a. Correlations in Direction (1,1), (2,2), and (3,3)

b. Spectra in Direction (1,1), (2,2), and (3,3)

Figure 12. Dryden Correlations and Closed Form Solution Spectra, ($L/V = 4.0$; $s/L = 0.20$).

have a sign change (positive to negative) which occurs at a value of z given by

$$z = \frac{2K_{5/6}(z)}{K_{1/6}(z)} \tag{21}$$

for von Karman and

$$z = \frac{2K_1(z)}{K_0(z)} \tag{22}$$

for Dryden.

Equations 21 and 22 vary as a function of the conditions under investigation, and for Figures 11 and 12 the sign changes at approximately $f = 0.5$. Since the absolute value of the spectra is plotted in order to preserve the log-log plot, the negative values appear as a lobe or spike. The concept of a negative spectrum value initially seems contra to physical reasoning. However, for turbulent fluctuations having wavelengths half the wing span, a positive velocity on one wing tip will correlate with a negative velocity on the other (see Figure 13) thus producing what appears as a negative turbulence kinetic energy.

It should also be noted that the limit of Equations 16 and 20 converges to the one-point spectra presented in the standard literature; i.e,

von Karman

$$E_{11}(\nu) = \frac{2}{[1 + (a\nu)^2]^{5/6}}$$

$$E_{ii}(\nu) = \frac{1 + (\frac{8}{3})(a\nu)^2}{[1 + (a\nu)^2]^{11/6}} \; , \; i = 2, 3$$

Dryden

$$E_{11}(\nu) = \frac{2}{1 + \nu^2}$$

$$E_{ii}(\nu) = \frac{1 + 3\nu^2}{[1 + \nu^2]^2} \; , \; i = 2, 3$$

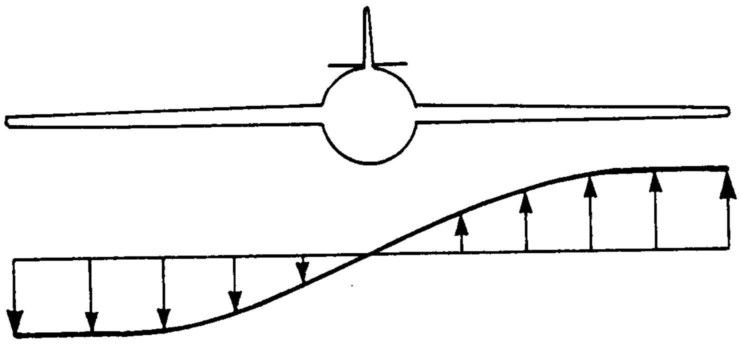

Figure 13. Half-Wave Length Distribution of Turbulent Fluctuations.

CHAPTER III

THE EFFECTS OF COMPUTING TWO-POINT SPATIAL SPECTRA FROM DIGITIZED DATA

The spectra resulting from atmospheric turbulence is generally computed from a digitized velocity fluctuation time history of finite length. This velocity fluctuation time history is processed through a Discrete Fourier Transform (DFT). The process of digitizing the data and only analyzing a finite time history creates aliasing and bias errors. In addition, when processing real data, variance errors will be induced because turbulence is a random function. Of these three primary error sources, only variance will not be discussed since it involves real data and each real data set is unique and can only meaningfully be treated as a specific entity and not as a general case.

Both bias and aliasing errors can be reduced, but never completely eliminated by appropriate computational techniques. These errors and the various means to reduce them can be understood using the correlations and analytical spectra described in Chapter II. The von Karman model is chosen for illustration purposes in this study because it best represents atmospheric data. The results of this chapter, however, apply equally well to the Dryden model. This closed form solution will be compared to various DFT solutions for the spectra computed from the digitized von Karman correlation. The graphical comparison of these two approaches will illustrate both aliasing and bias errors and the success or lack there of in reducing them.

In order to use meaningful values of L/V and s/L for this analysis a specific set of realistic conditions was selected based on a Boeing 747-400 type aircraft which has a wing span of 196 ft (60 m). This aircraft has a landing speed of 165.0 mph or

75.0 m/sec. In addition, a representative length scale for atmospheric turbulence of 990 ft (300 m) was assumed. The above stated conditions result in the following ratios

$$\begin{aligned} s/L &= 0.20 \\ L/V &= 4.00 \end{aligned} \tag{23}$$

A. The Discrete Fourier Transform

The Discrete Fourier Transform (DFT) is defined in Oppenheim and Schafer (1975) as the Fourier representation of a finite-duration periodic sequence. In this reference the DFT is represented by the following transform pair

$$X(k) = \begin{cases} \sum_{n=0}^{N-1} x(n)\, e^{-j2\pi k\, n/N}, & 0 \le k \le N-1 \\ 0 & \text{otherwise} \end{cases} \tag{24}$$

$$x(n) = \begin{cases} \frac{1}{N} \sum_{k=0}^{N-1} X(k)\, e^{j2\pi k\, n/N}, & 0 \le n \le N-1 \\ 0 & \text{otherwise} \end{cases} \tag{25}$$

where $x(n)$ is a finite-duration sequence and $X(k)$ is the Fourier transform of this sequence. It must be noted that where DFT relations are concerned, a finite-duration sequence is considered to be one period of a periodic sequence.

In order to determine the frequency content of the finite-duration sequence, at least two samples per cycle are required. If data is sampled at an interval of τ, then there are $1/\tau$ samples per second. The highest frequency that can be defined by $1/\tau$ samples per second is $1/(2\tau)$ Hz. Any energy contained in higher frequencies in the sequence will be folded back or aliased into the energy contained in the frequency range 0 to $1/(2\tau)$ Hz. The point at where the aliasing begins is known as the Nyquist Frequency, f_N. The effect of folding or aliasing is illustrated graphically in Figure 14b from Oppenheim and Schafer (1975).

Consider the Fourier transform $E(\omega)$ of a continuous time function given in Figure 14(a) and the DFT, $E^T(\omega)$ for the discrete time version of the same function

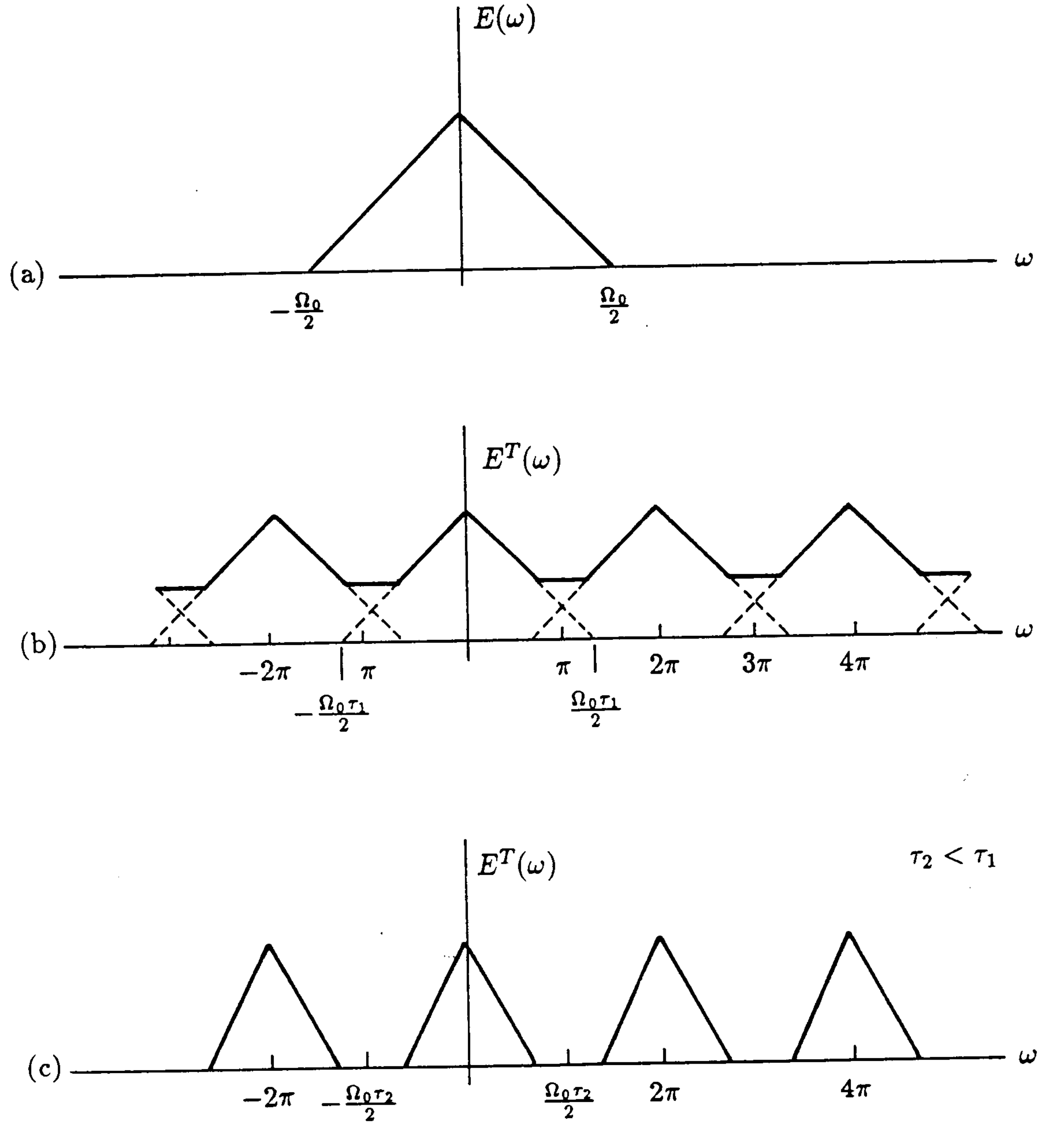

Figure 14. (a) Fourier Transform of Continuous-Time Signal.
(b) Fourier Transform of the Discete-Time Signal Obtained by Periodic Sampling. The sampling period is large, so the periodic repetitions of the continuous-time transform overlap.
(c) Same as (b), but with the sampling period small enough so that the periodic repetitions of the continous-time transform do not overlap. (Oppenheim and Schafer (1975)).

given in Figure 14(b). The period of $E(\omega)$ is Ω_0 and the sampling interval is τ_1. In Figure 14(b) the period of the function $E^T(\omega)$ is defined such that

$$\Omega_0 > 2\pi/\tau_1 \tag{26}$$

This means that the sampling period is too large and causes the $E^T(\omega)$ to be shifted such that they overlap. This phenomenon is aliasing and causes high-frequency energy to, in effect, be added to lower frequency energy.

The second major type of error introduced from using the DFT technique occurs due to analyzing a finite duration of the total sequence. This is called bias error. Bias error occurs because the DFT analyses treats the finite-duration sequence as one period of a periodic sequence. Since at least two sampling periods are required to recover the frequency content of the sample, the DFT process reflects the finite sample of discrete data points about an end point. This assumes that the finite sample of discrete data is a single period of a periodic function. When the data sample is not periodic as the example from Harris (1978) shown in Figure 15, a bias error occurs. This error source is also known as spectral leakage and/or truncation error.

Calculation of atmospheric turbulence spectra is generally carried out by direct Fourier transform of measured digitized turbulent velocity time history. Aliasing and bias errors are thus inherent in the resulting spectra. In most reported results, procedures to avoid aliasing errors are carefully implemented. Generally however, limited consideration is given to bias error. Frost, et al. (1987) observe that for one-point or auto-spectra, aliasing is the major contributor to error but for two-point spectra bias error is by the most significant. Their observation was based on limited investigation. In the following sections a more indepth investigation into the nature of aliasing and bias error is presented and procedures for reducing bias error are given.

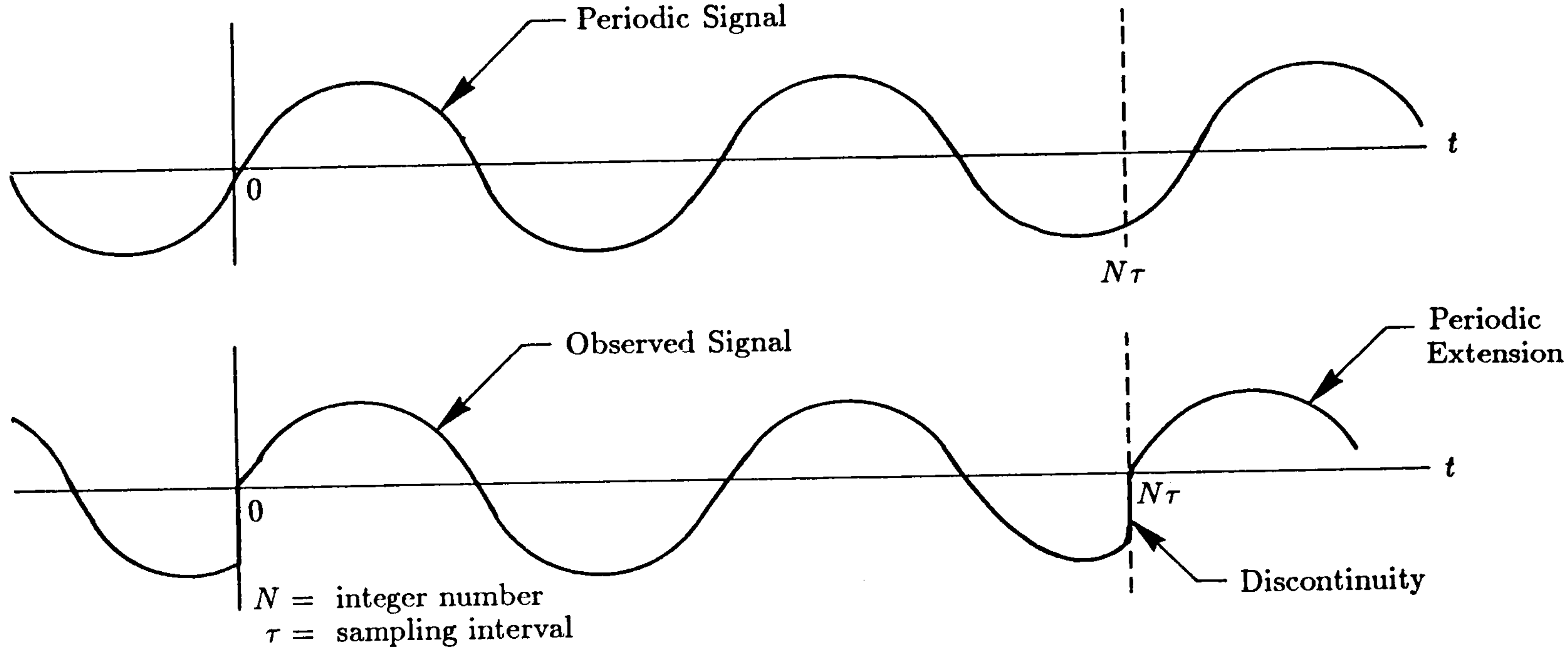

Figure 15. Periodic Extension of a Sinusoid Which is not Periodic in the Observation Interval (Harris (1978)).

The investigation of errors introduced by the DFT technique is carried out by digitizing the von Karman (Equation 15) and Dryden (Equation 18) correlations. The DFT is then applied to compute the spectra. The DFT values are then compared with the closed form analytical spectra. Departures of DFT results from the closed form solution are a measure of the aliasing error introduced by the selected digitizing time step Δt and of the bias error introduced by truncating the correlations at specified time periods. The results of investigating errors by the above described procedure is illustrated in Figures 16, 17, and 18.

Figures 16a, 17a, and 18a present the one-point spectra with the solid lines representing the closed form solutions for the von Karman spectra for velocity components in the directions 1, 2 and 3, respectively. The closed form solutions are the auto-spectra given by Equation 16. The dashed lines represent the spectra resulting from the DFT technique applied to Equations 15 for three truncation lengths of 6.4 sec. (256 points), 12.8 sec. (512 points), and 51.2 sec. (2048 points), respectively. A sampling rate of 40 samples per second (i.e., $\tau = 0.025$ sec.) was employed which, in principle, will resolve all frequencies up to 20 Hz. The plotted results clearly show aliasing errors which become highly visible at approximately 5 Hz. Further inspection of the figures shows that extending the length of the digitized correlation data record from 256 points to 2048 points while holding the sampling rate at 40 Hz, has no effect on the DFT solution of the auto-spectra. This indicates that truncating the record length before using the DFT (i.e., bias error) is not a major error source and that the error in the auto-correlation is primarily from aliasing.

Aliasing is reduced by sampling the data sequence at a higher rate. In Figure 19, the data were sampled 80 samples/sec. or ($\tau = 0.0125$ sec.) twice the rate used for Figures 16, 17, and 18. Thus, the folding frequency is now 40 Hz as contrasted to 20 Hz. As can be seen from this figure, the DFT solutions based on the higher

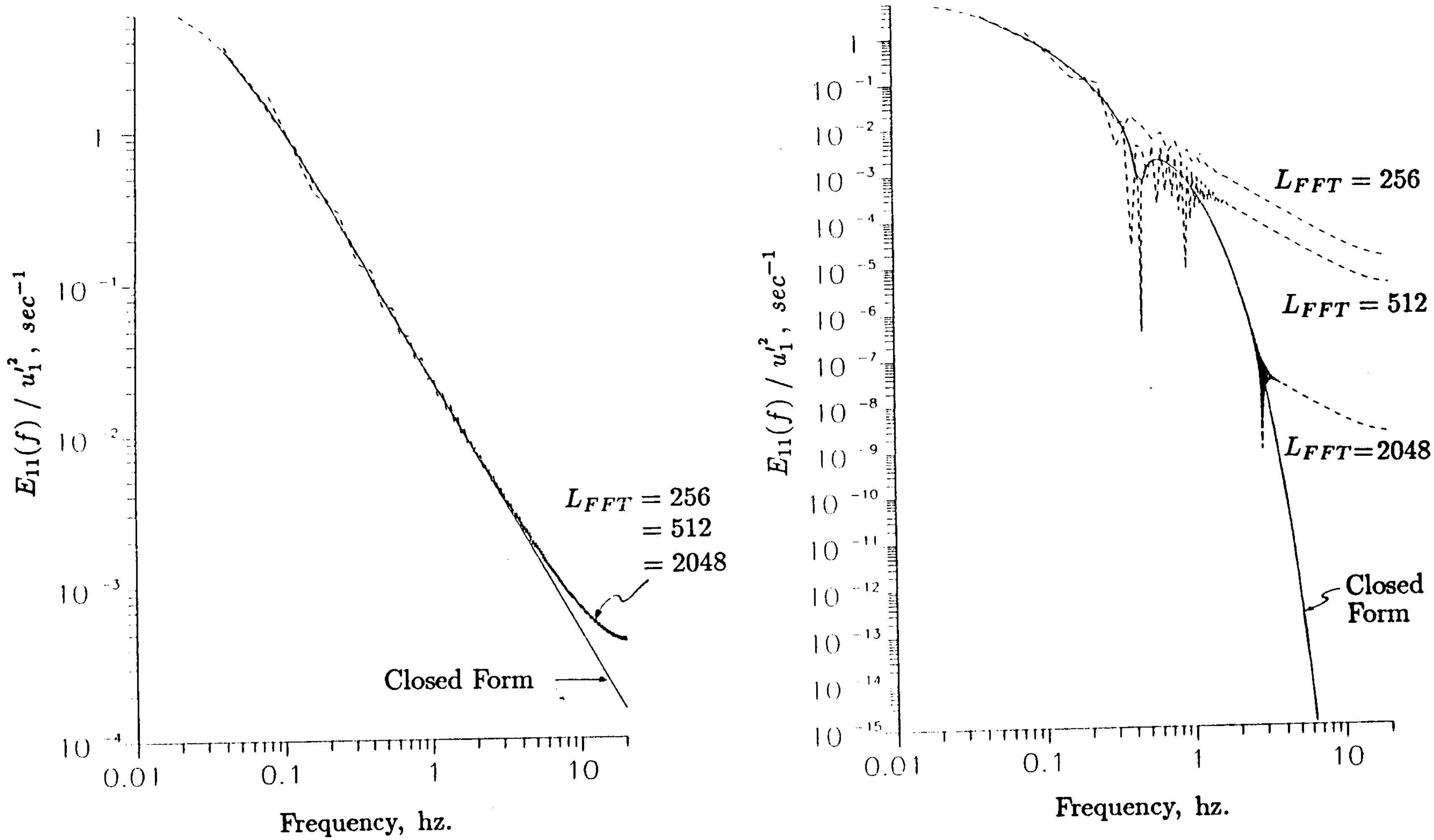

a. Spectra in Direction (1,1) for $s/L = 0.00$

b. Spectra in Direction (1,1) for $s/L = 0.20$

Figure 16. Effects of Finite Record Length (von Karman Closed Form and DFT Solutions, $L/V = 4.0$).

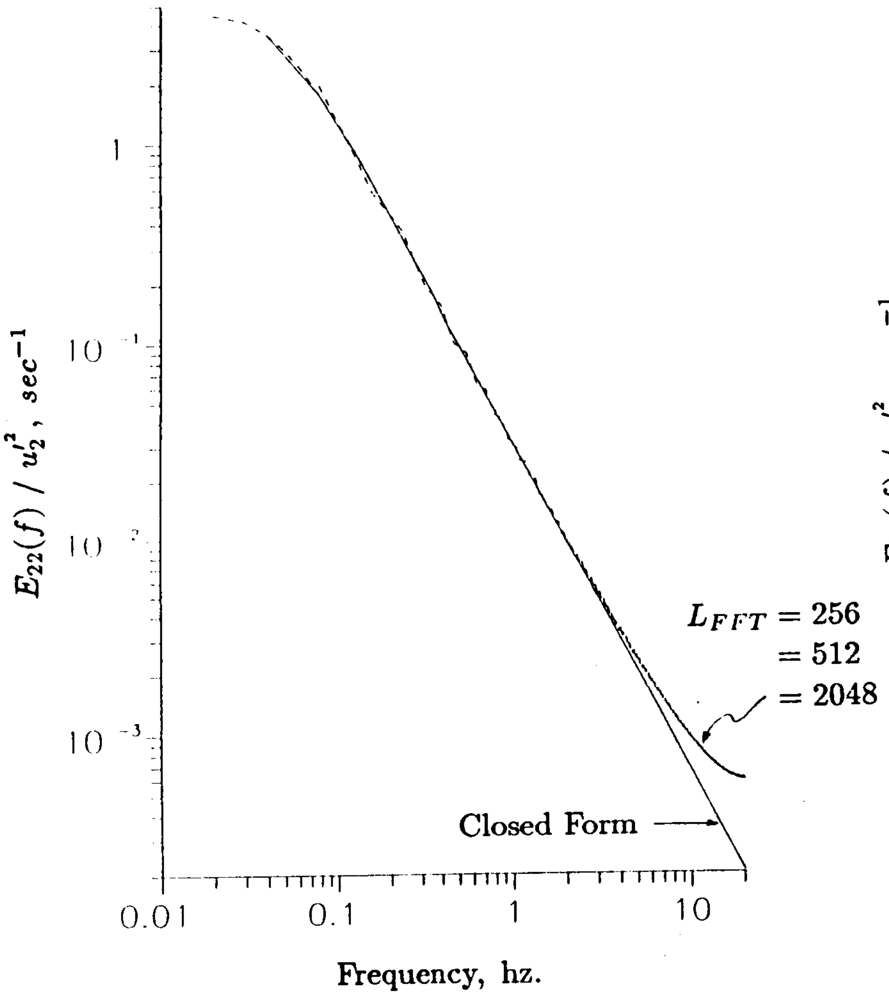

a. Spectra in Direction (2.2) for $s/L = 0.00$

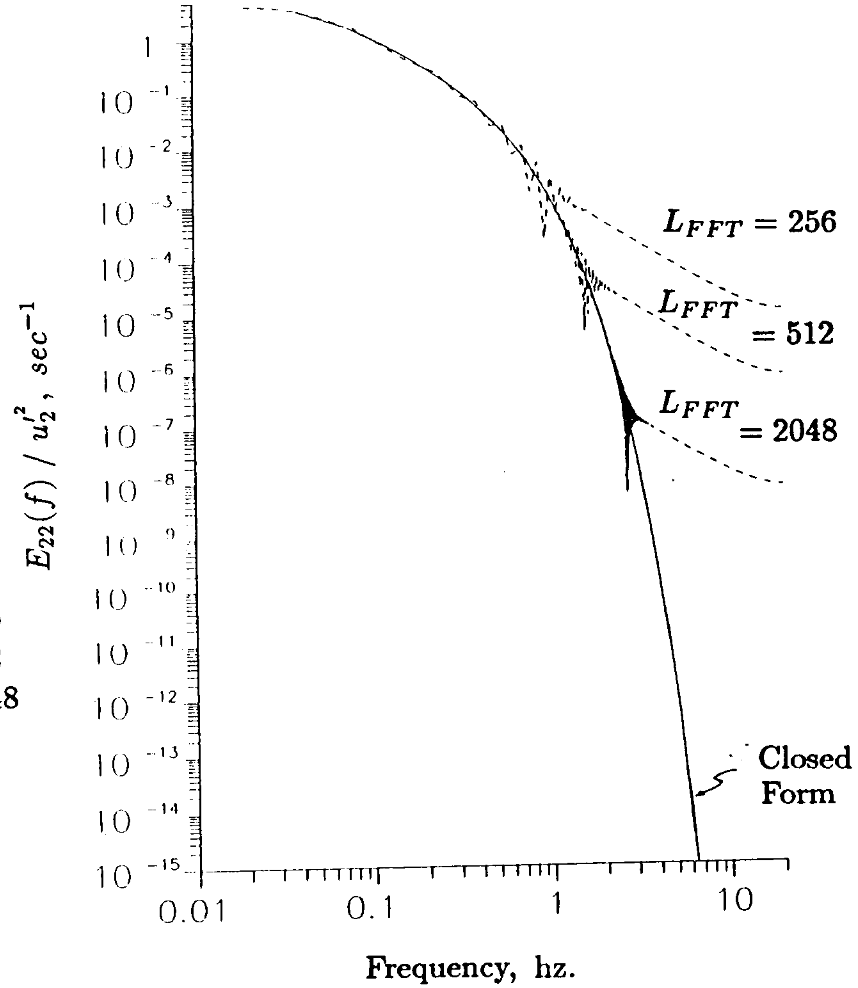

b. Spectra in Direction (2.2) for $s/L = 0.20$

Figure 17. Effects of Finite Record Length on von Karman Closed Form and DFT Solutions, $(L/V = 4.0)$.

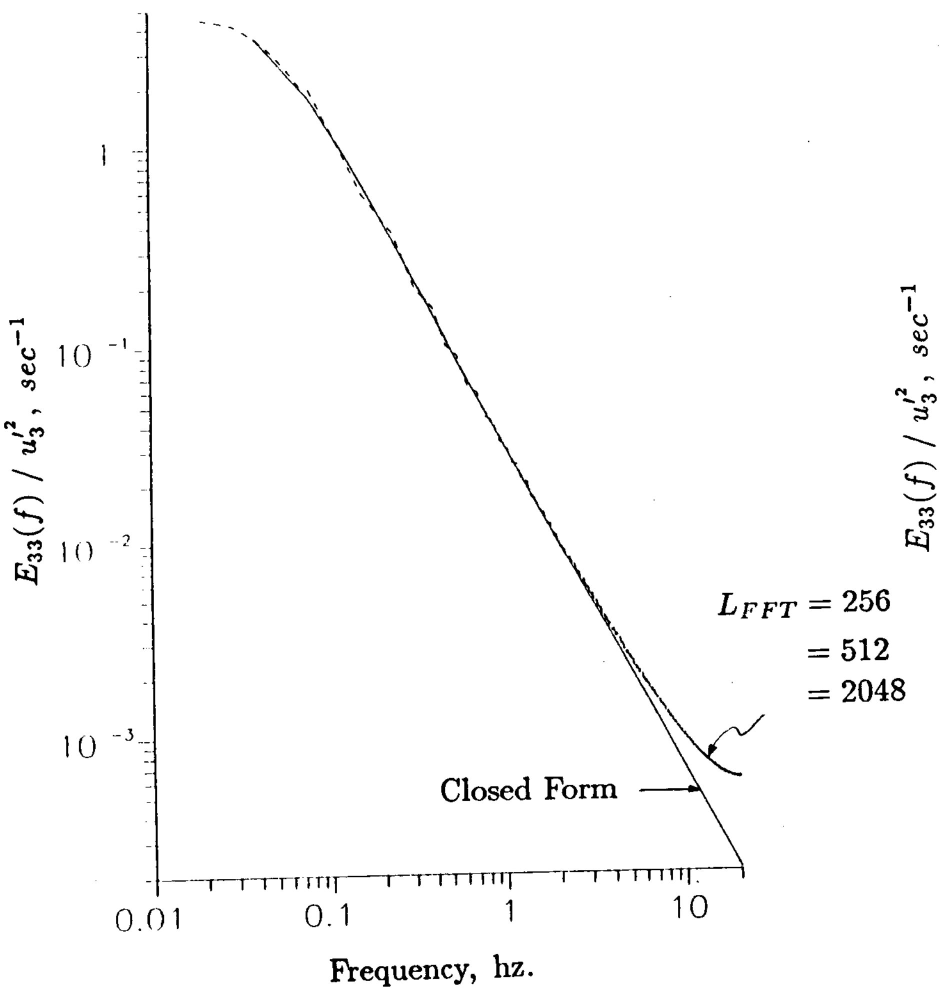

a. Spectra in Direction (3,3) for $s/L = 0.00$

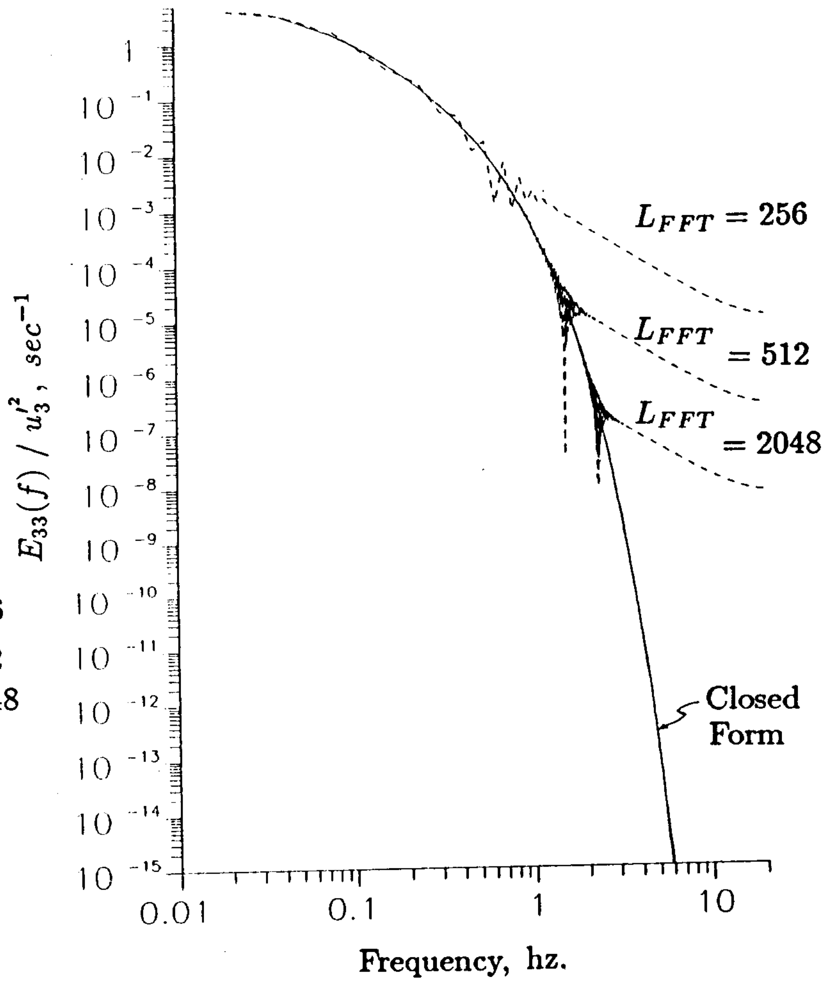

b. Spectra in Direction (3,3) for $s/L = 0.20$

Figure 18. Effects of Finite Record Length on von Karman Closed Form and DFT Solutions, $(L/V = 4.0)$.

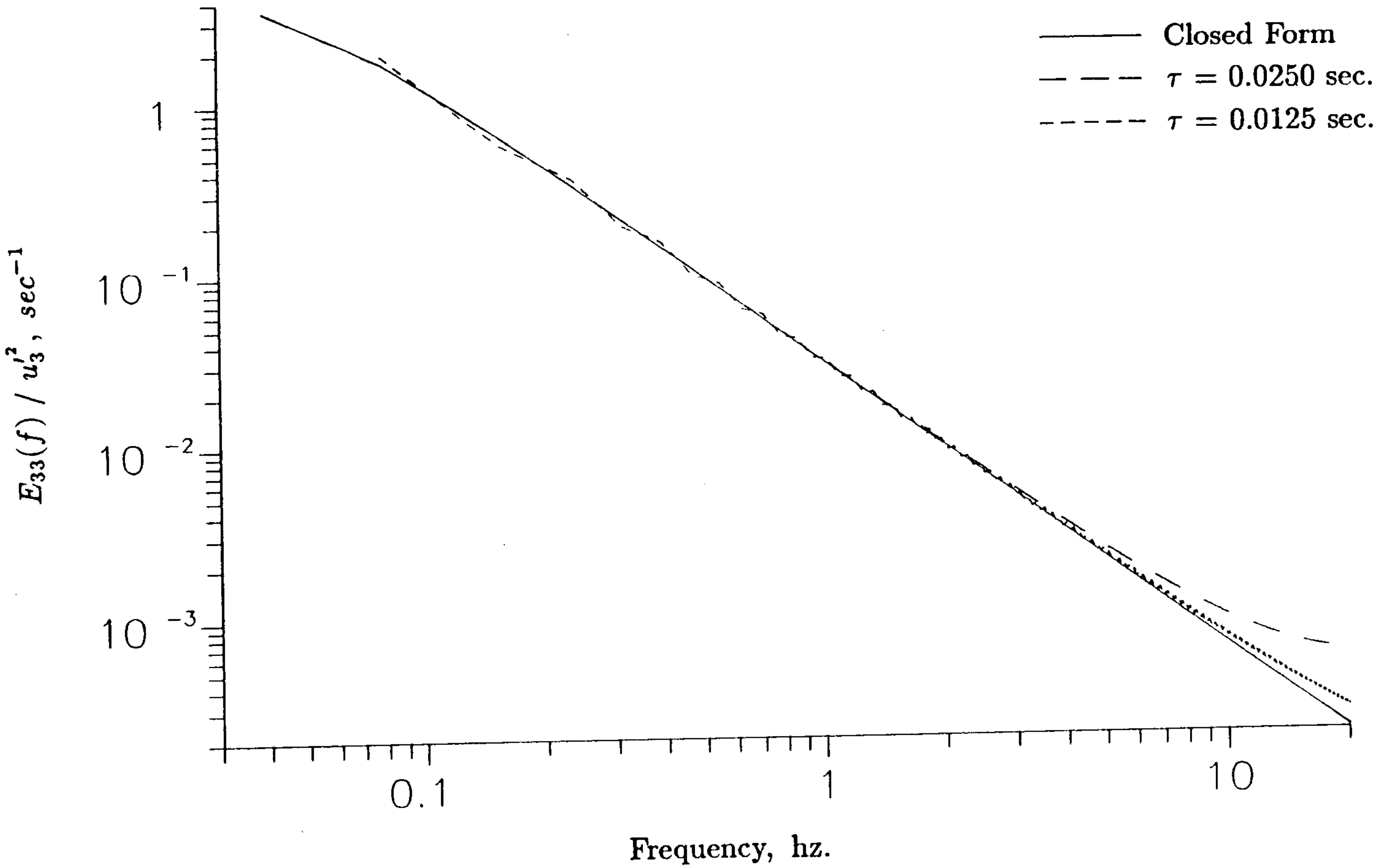

Figure 19. Effects of Sample Rate on Aliasing ($L/V = 4.0; s/L = 0.00$).

sampling rate much closer follows the closed form solution than the solutions for the lower sampling rate.

Now re-examine part b of Figures 16, 17, and 18 which is a plot of two-point spectra computed with a DFT of the digitized form of Equation 15 compared with the closed form Equation 16. It is readily apparent that the record or truncation length has a pronounced effect on the DFT solutions. These figures clearly indicate the significance of bias error which occurs when DFT techniques are applied to computation of two-point spatial spectra.

Aliasing errors in the two-point spectra are not obvious in Figures 16b, 17b, and 18b. To further examine the magnitude of aliasing error the DFT solutions for a fixed sample length of 512 points and for digitizing increments of $\tau = 0.025$ sec. and 0.1 sec., respectively, are shown. For the 0.025 sec. case, a frequency content of up to 20 Hz can be resolved where as for the 0.100 sec. case, the maximum resolvable frequency is 5 Hz. As can be seen in both Figures 20a and 20b which are the von Karman spectra in directions 3 and 1, respectively. Interestingly, the data for the largest digitizing increment $\tau = 0.1$ sec. fits the closed form solution to higher frequencies better than the 0.025 sec. results. The observation is deceptive, however, because the number of data points is fixed at 512, thus case one ($\tau = 0.025$ sec.) is for a total time of 12.8 seconds whereas case two ($\tau = 0.1$ sec.) is for a time of 51.2 seconds. Therefore, it is actually the bias error which is observed and not an aliasing error. Figure 21 illustrates this effect further. In this figure, the correlation function for direction 1 is plotted as a function of time. The cut-off times for both case 1 and case 2 are shown. It can be seen that for case one, which terminates at 12.8 seconds, the correlation is much further from zero than for case two which terminates at 51.2 seconds. A sample length of 2048 points would be required at a time interval of 0.025 seconds (i.e., case 1) to reduce the bias error to

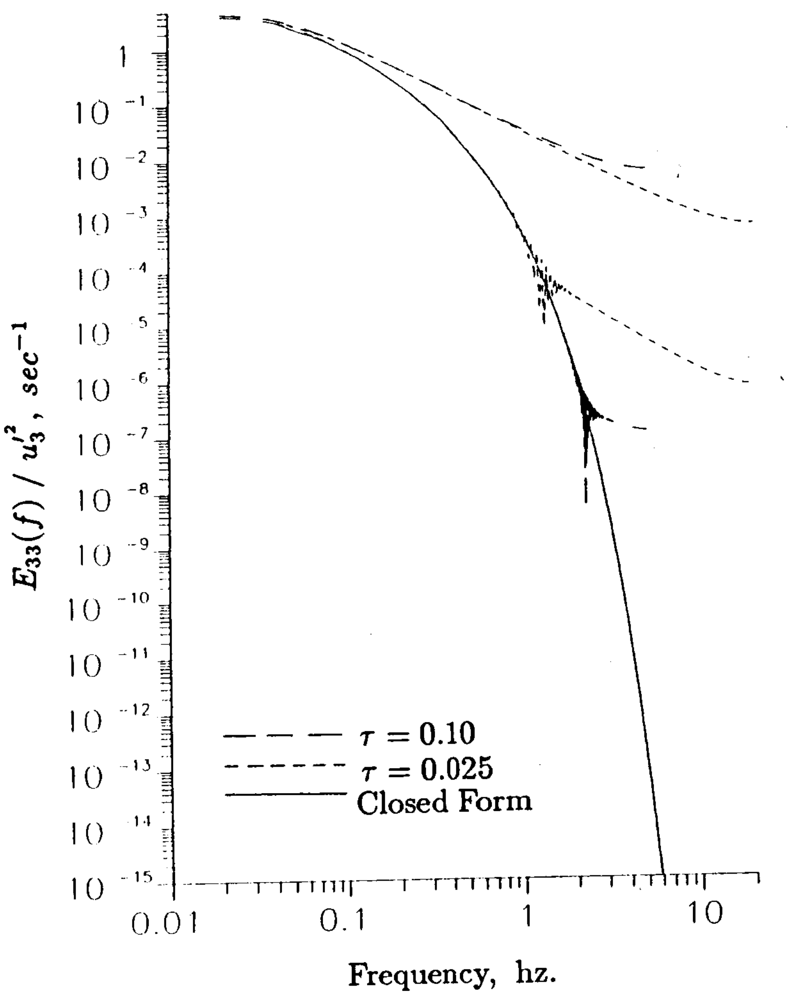

a. Spectra in Direction (3,3)

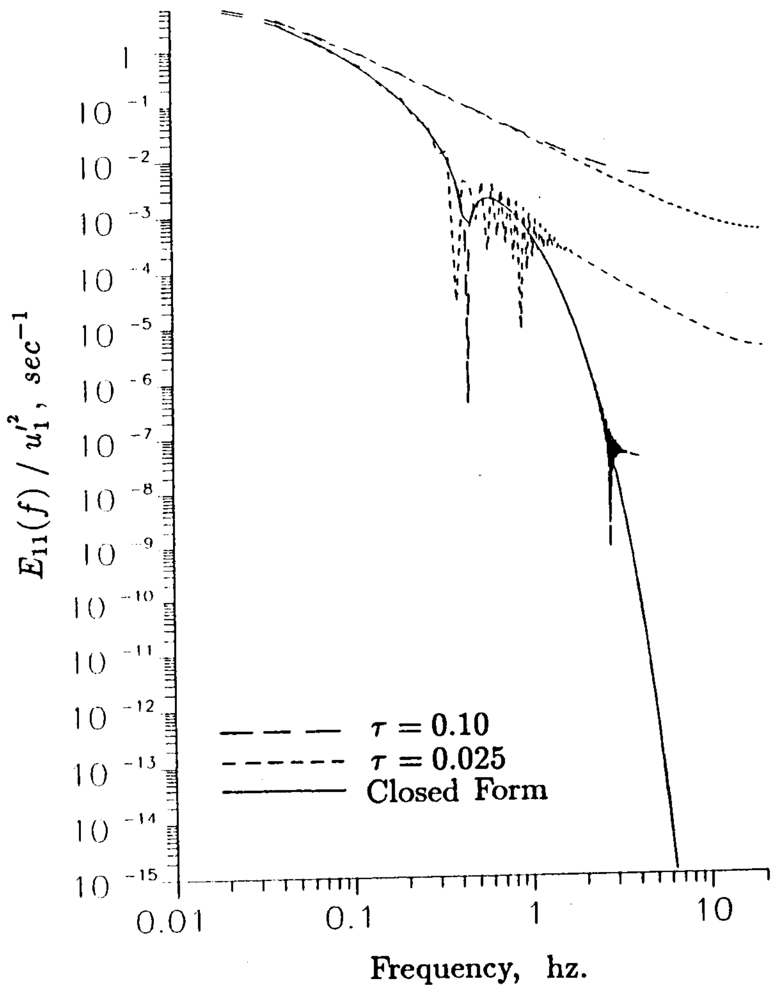

b. Spectra in Direction (1,1)

Figure 20. Effects of Digitized Increment on the von Karman Closed Form and DFT Solutions, ($L/V = 4.0$; $s/L = 0.20$; $L_{FFT} = 512$).

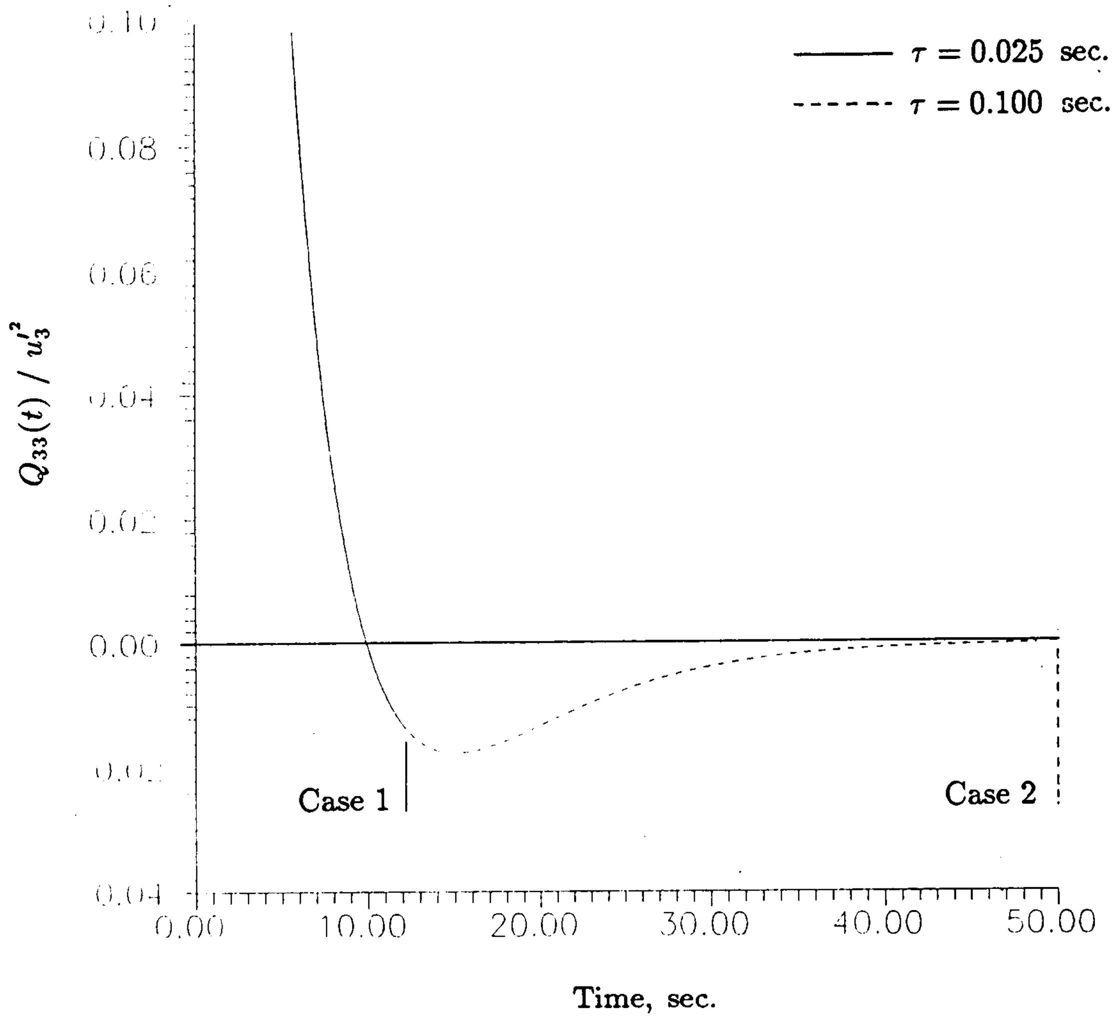

Figure 21. Error Introduced by Truncating Correlation Sample (512 points).

the same level as for case two. Therefore the analyst must trade off bias error for frequency content in establishing test data collection criteria.

In Figure 22 the effect of changing the correlation separation ratio from 0.0 (auto-correlation with no separation) to twice the characteristic length scale of the turbulence $s/L = 2.0$ can be seen. In this figure both the direction 1 spectra, Figure 20a, and the direction 3 spectra, Figure 20b, are shown. At a certain point, the DFT solutions diverge from the closed-form solution due to lobing or the influence of truncation. At the divergent point, a "ringing" or instability occurs due to the inherent side-lobe structure. The side-lobe structure is strongly dependent on the manner in which the correlation is truncated. If the correlation is simple set to zero for all values after the truncation length, the DFT is said to have a rectangle window. The influence of a rectangle, as well as other windows, are discussed in the next section.

B. Window Functions

Window functions can be used to reduce the bias errors resulting from truncation. For two-point spatial spectra computed from the correlation models given by either Equation 15 or Equation 18, windowing consists of multiplying the correlation function with a prescribed function (called a window function) prior to computing the DFT. For example, given the window function $W(t)$, Equation 13 becomes

$$(E_{i,j})_{A,B} = \int_{-\infty}^{\infty} W(t)\ (Q_{i,j})_{A,B}\ e^{-i\omega t}\ dt \tag{27}$$

or in the DFT form

$$(E_{i,j})_{A,B} = \sum_{n=0}^{N-1} W(nt)\ (Q_{i,j})_{A,B}\ e^{-j\omega nT} \tag{28}$$

The most basic form of the window function $W(t)$ is the rectangle window where

$$W(n) = \begin{cases} 1.0, & n = 0, 1, \ \ldots, \ N-1 \\ 0 & n > N-1 \end{cases} \tag{29}$$

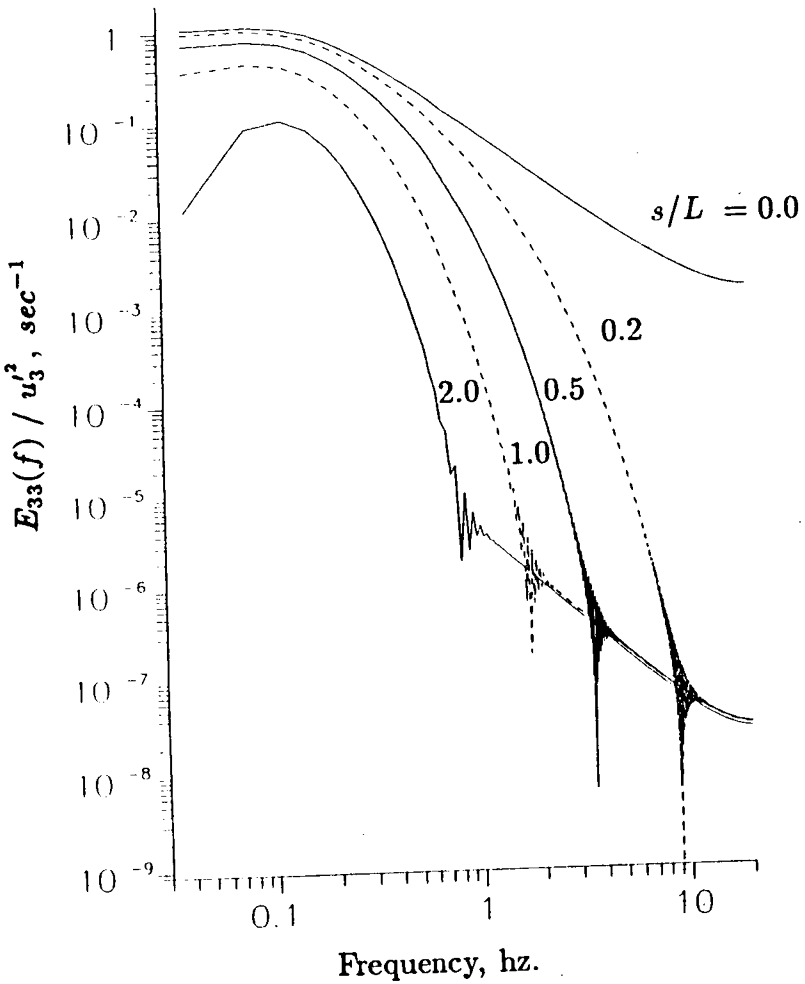

a. Spectra in Direction (3,3)

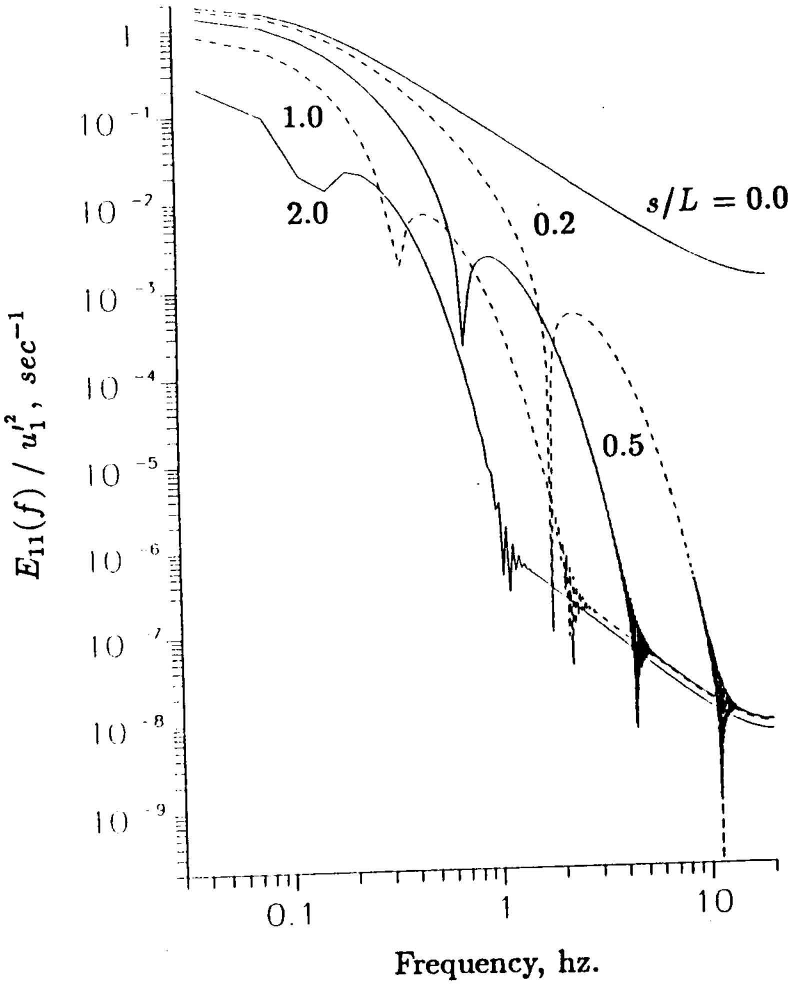

b. Spectra in Direction (1,1)

Figure 22. DFT Spectra Computed From the von Karman Correlation ($L/V = 1.0$; $L_{FFT} = 512$).

This function (shown graphically in Figure 23) can be thought of as a unit gating function applied over the data interval. The rectangle window also known as the Dirichlet window is used by default when all of the data points in a finite length sample are weighted equally.

Another standardly used window is the triangle or Bartlett window also shown in Figure 23. The triangle window for a DFT is defined as

$$W(n) = \begin{cases} 1.0 - \frac{n}{N/2} & , \quad n = 0, 1, \ldots, \frac{N}{2} \\ W((N-n)) & , \quad n = -\frac{N}{2}, \ldots, N-1 \\ 0 & , \quad |n| > \frac{N}{2} \end{cases} \tag{30}$$

For both the rectangle and triangle window, the log-magnitude of the Fourier transform of the window function $W(t)$ have the forms presented in Figure 24 (Harris (1978)). The side-lobe structure of the window functions is clearly shown in this figure.

Papoulis (1977) points out that although there are many extensively used windows beyond the basic two windows described above, and that while these other windows have good overall properties, most of them have not been optimized for any specific set of conditions. Papoulis (1977) develops a proof that the Bohman window defined by the equation

$$\begin{gathered} W(n) = \left[1.0 - \frac{|n|}{N/2}\right] cos\left\{\pi \frac{|n|}{N/2}\right\} + \frac{1.0}{\pi}\, sin\left\{\pi \frac{|n|}{N/2}\right\}, \\ 0 \leq |n| \leq \frac{N}{2} \end{gathered} \tag{31}$$

will minimize the truncation error in high-resolution computations. He uses a moment expansion to prove that the error is minimum if the second derivative of $E(\omega)$ is a minimum. The Bohman window is referred to by Papoulis as a minimum amplitude moment window or simply the minimum moment window. Papoulis strongly recommends its use when trying to eliminate bias or truncation errors. The min-

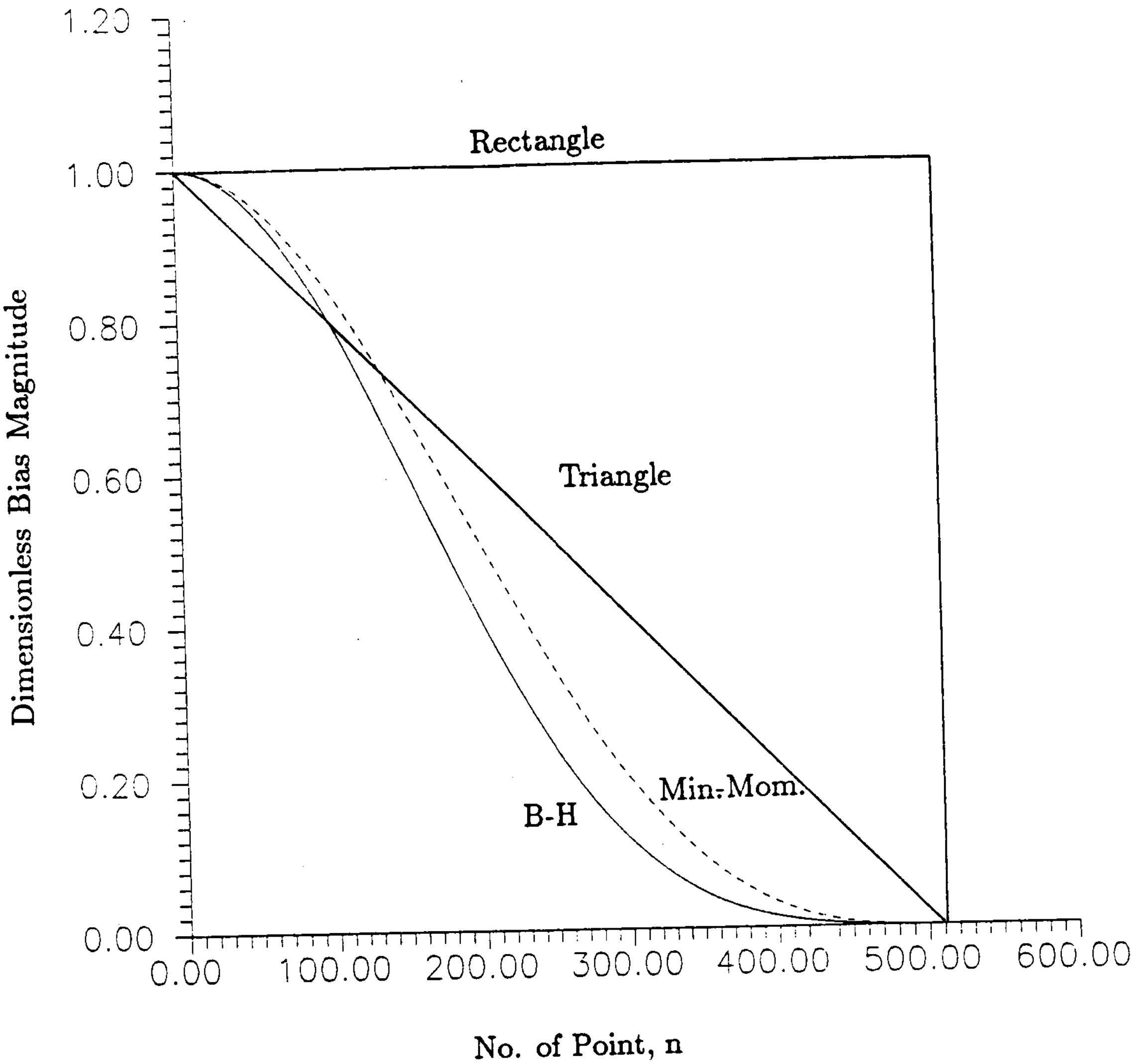

Figure 23. Weighting Associated with Four Different Window Functions.

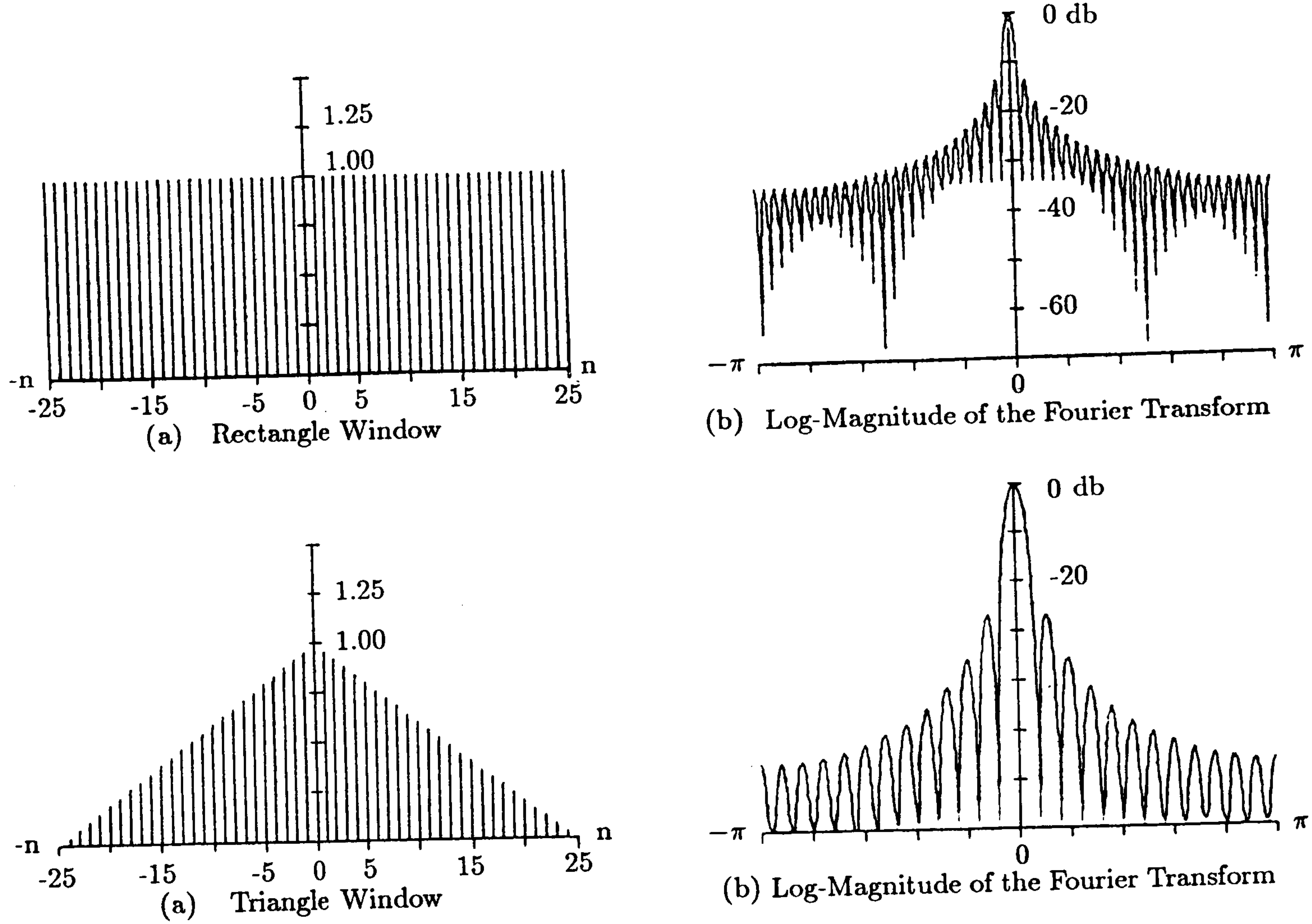

(a) Rectangle Window

(b) Log-Magnitude of the Fourier Transform

(a) Triangle Window

(b) Log-Magnitude of the Fourier Transform

Figure 24. Basic Window Functions and Their Fourier Transforms.

imum moment window is one of the two optimum windows used in the remainder of this analysis.

The other optimum window comes from Harris (1978). Harris has developed a comprehensive catalog of available windows and tabulates significant performance parameters by which different windows can be compared. Harris selects optimum windows based on their ability to minimize side-lobes. He points out that the highest side-lobe of the 4-sample Blackman-Harris window function is -92db. This window is defined by the equation

$$W(n) = a_0 + a_1\ cos\left\{\frac{2\pi}{N}\ n\right\} + a_2\ cos\left\{\frac{2\pi}{N}\ 2n\right\} + a_3\ cos\left\{\frac{2\pi}{N}\ 3n\right\} \tag{32}$$

where

$$n = 0, 1, 2, \ldots, N-1$$

$$a_0 = 0.35875$$

$$a_1 = 0.48829$$

$$a_2 = 0.14128$$

$$a_3 = 0.01168$$

Figure 25 presents both the shape of the minimum moment window and the 4-term Blackman-Harris window along with their respective log-magnitude Fourier transforms. Note the difference in the side-lobe structures in going from the rectangle window in Figure 24 to the Blackman-Harris window in Figure 25. Table 1 (Harris (1978)) presents a comparison of some of the more important parameters of the four windows described in the preceding paragraphs. Figure 23 presents the weighting effect of the four window functions for each point in a 512 point data sample for the four windows used in this analysis. Again, inspecting Figure 25, note the difference in the side-lobe structure between the minimum moment win-

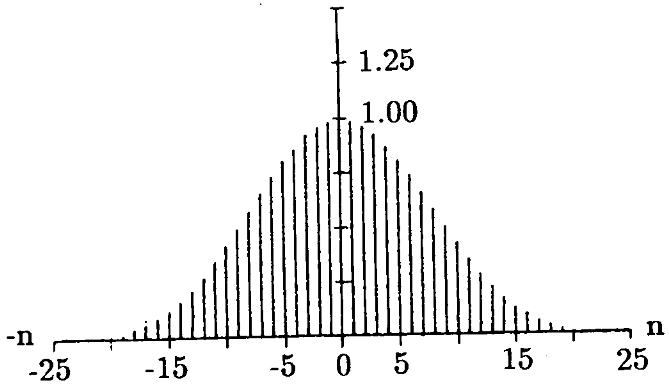

(a) The Minimum Moment Window

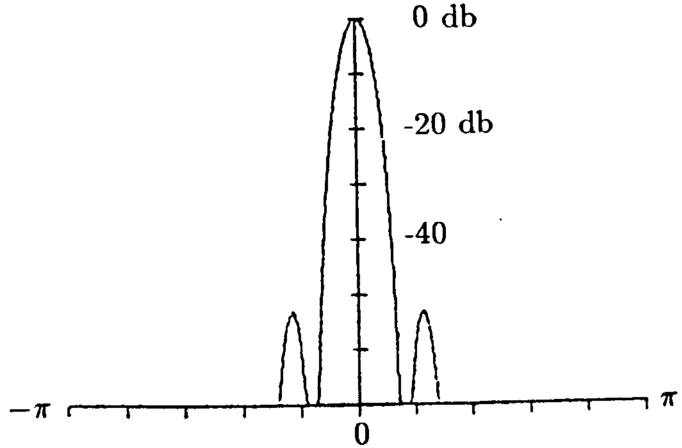

(b) Log-Magnitude of the Fourier Transform

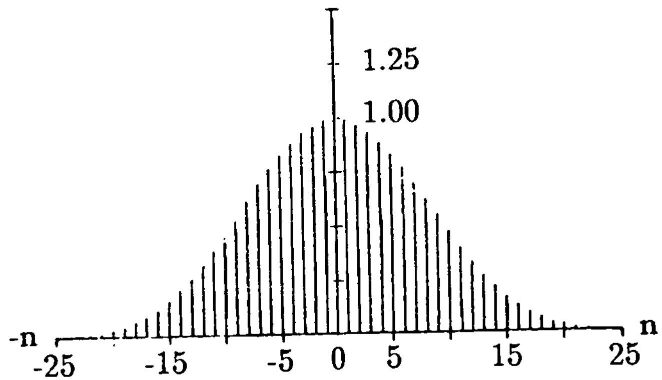

(a) 4-Term Blackman-Harris Window

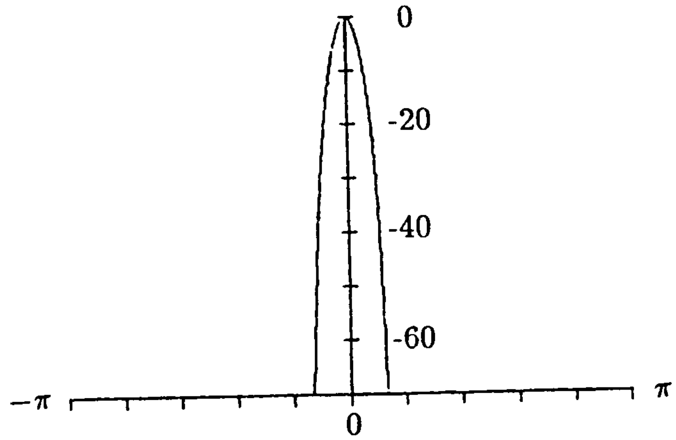

(b) Log-Magnitude of the Fourier Transform

Figure 25. Optimum Window Functions and Their Fourier Transforms.

TABLE 1. WINDOWS FOR REDUCING BIAS ERROR DUE TO RECORD LENGTH TRUNCATION (Harris (1978))

WINDOW	HIGHEST SIDELOBE LEVEL db	SIDELOBE FALLOFF (db/OCT)	EQUIV. NOISE BW (BINS)	3.0-db BW (BINS)	6.0-db BW (BINS)
Rectangle	-13	-6	1.00	0.89	1.21
Triangle	-27	-12	1.33	1.28	1.78
Bohman Minimum Moment	-46	-24	1.79	1.71	2.38
Minimum 4-Sample Blackman-Harris	-92	-6	2.00	1.90	2.72

dow function and the Blackman-Harris window function and then note in Figure 23 the small difference in the weighting between the two windows.

All four window functions were applied to the DFT solution for the von Karman two-point spatial spectra for the Boeing 747-400 type aircraft at landing speeds. A 512 sample data set was used with a digitizing interval of 0.025 seconds. Figures 26 through 28 compare the closed form solution and the DFT solutions with each of the respective windows. The figures are for direction 1, 2, and 3, respectively. In these figures the rectangle and triangle windows result in the form of DFT solutions generally presented in the literature. The minimum moment solution proposed by Papoulis (1977), however, does in fact, reduce the bias error and allow the DFT solution to better approximate the closed form solution. It is, however, very obvious that the 4-term Blackman-Harris window gives even better reduction of the bias error. The reduction produced by the Blackman-Harris window over that produced with the minimum moment window is equivalent to the reduction that the minimum moment window gives over the rectangular window. These results were consistent for all cases investigated.

The side-lobe structure of the window is the primary parameter controlling the results of windowing. It is apparent from Figure 26 through 28 that a triangle window degrades the two-point spectra computed with the DFT more than any of the other windows. Analysts computing two-point spectra of atmospheric turbulence should therefore refrain from using a Bartlett window. It is, in fact, strongly recommended that either the minimum moment or preferably the Blackman-Harris windows be used.

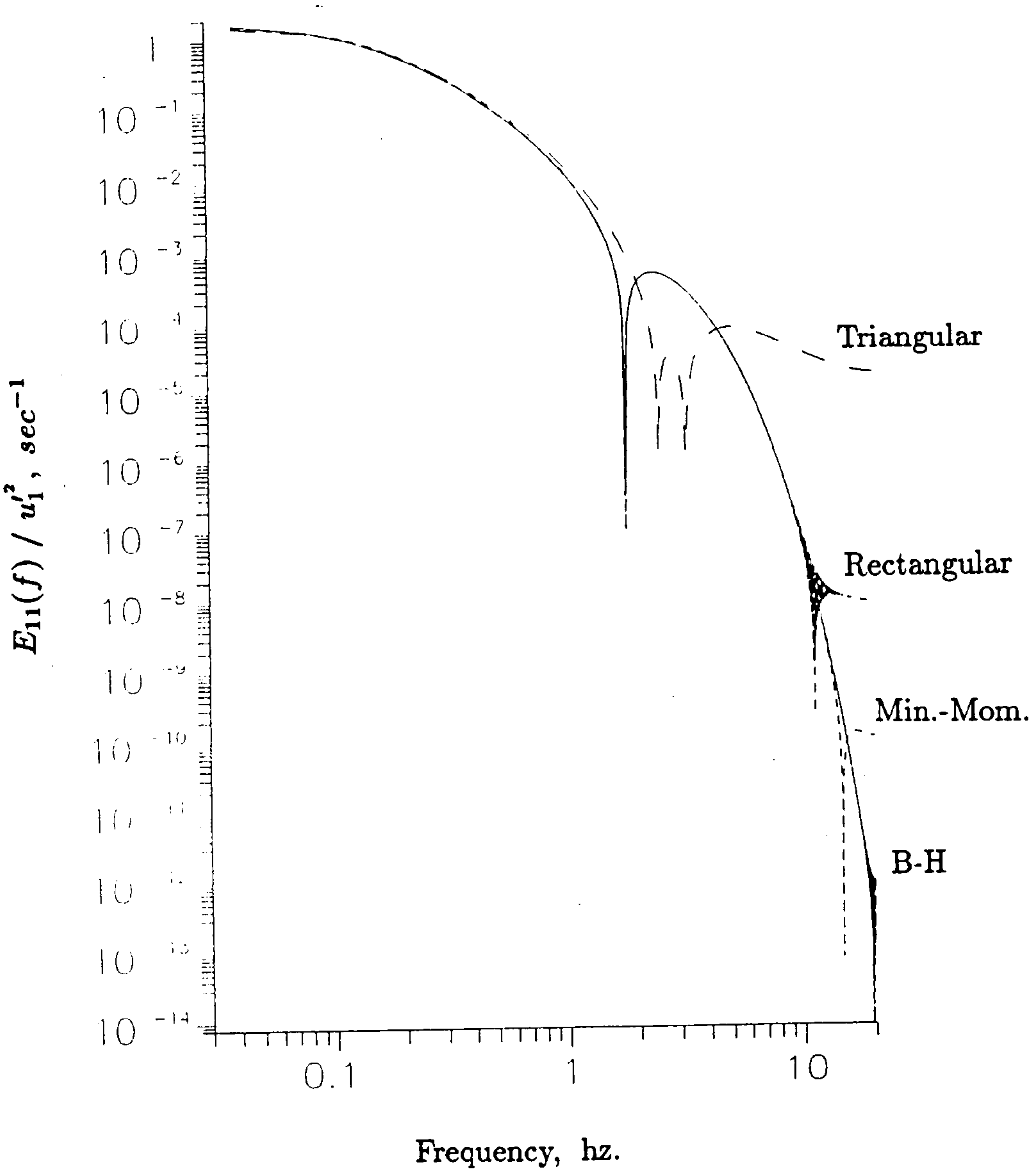

Figure 26. Effects of Windowing on the von Karman Spectrum in Direction (1,1) ($L/V = 4.0$; $s/L = 0.2$; $L_{FFT} = 512$).

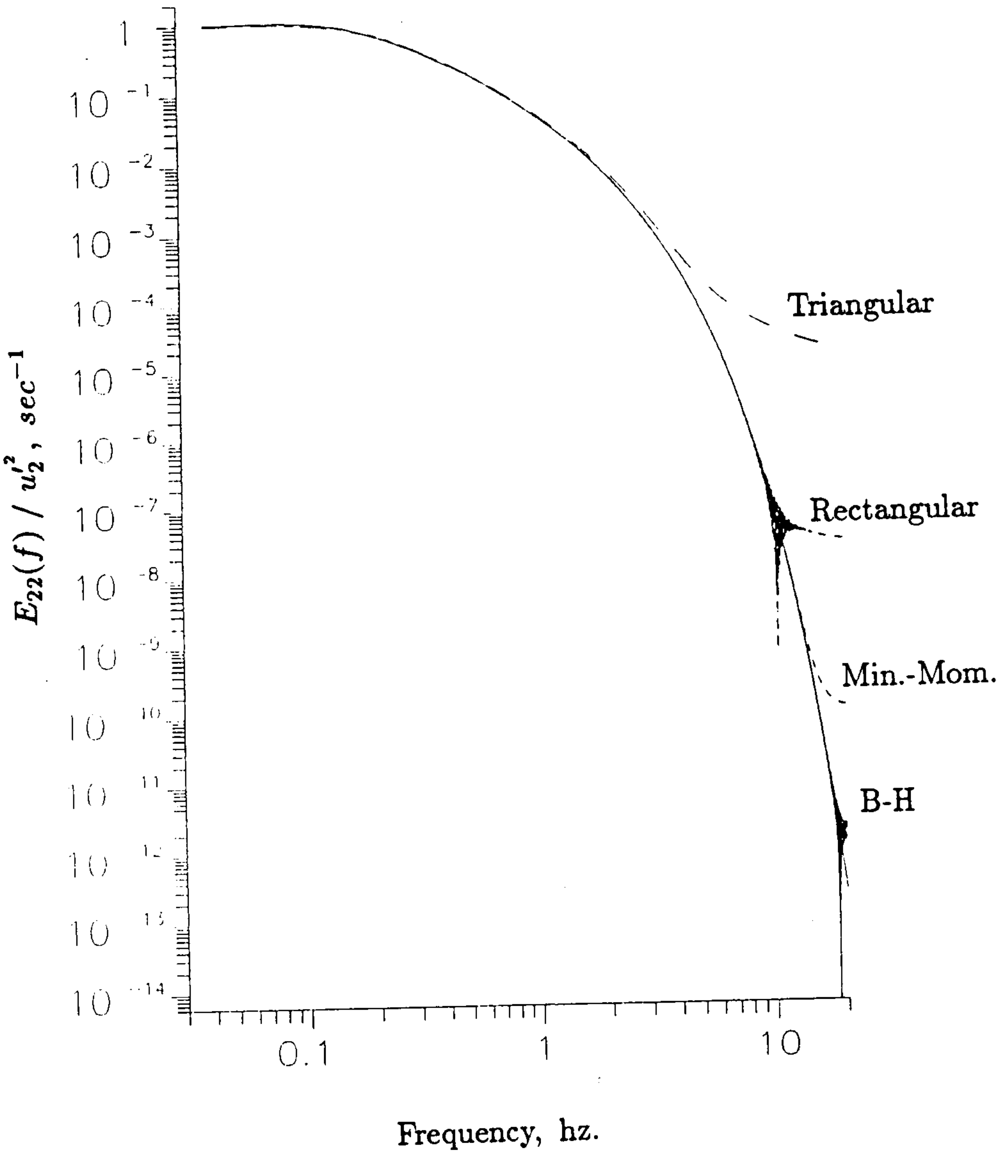

Figure 27. Effects of Windowing on the von Karman Spectrum in Direction (2,2) ($L/V = 4.0$; $s/L = 0.2$; $L_{FFT} = 512$).

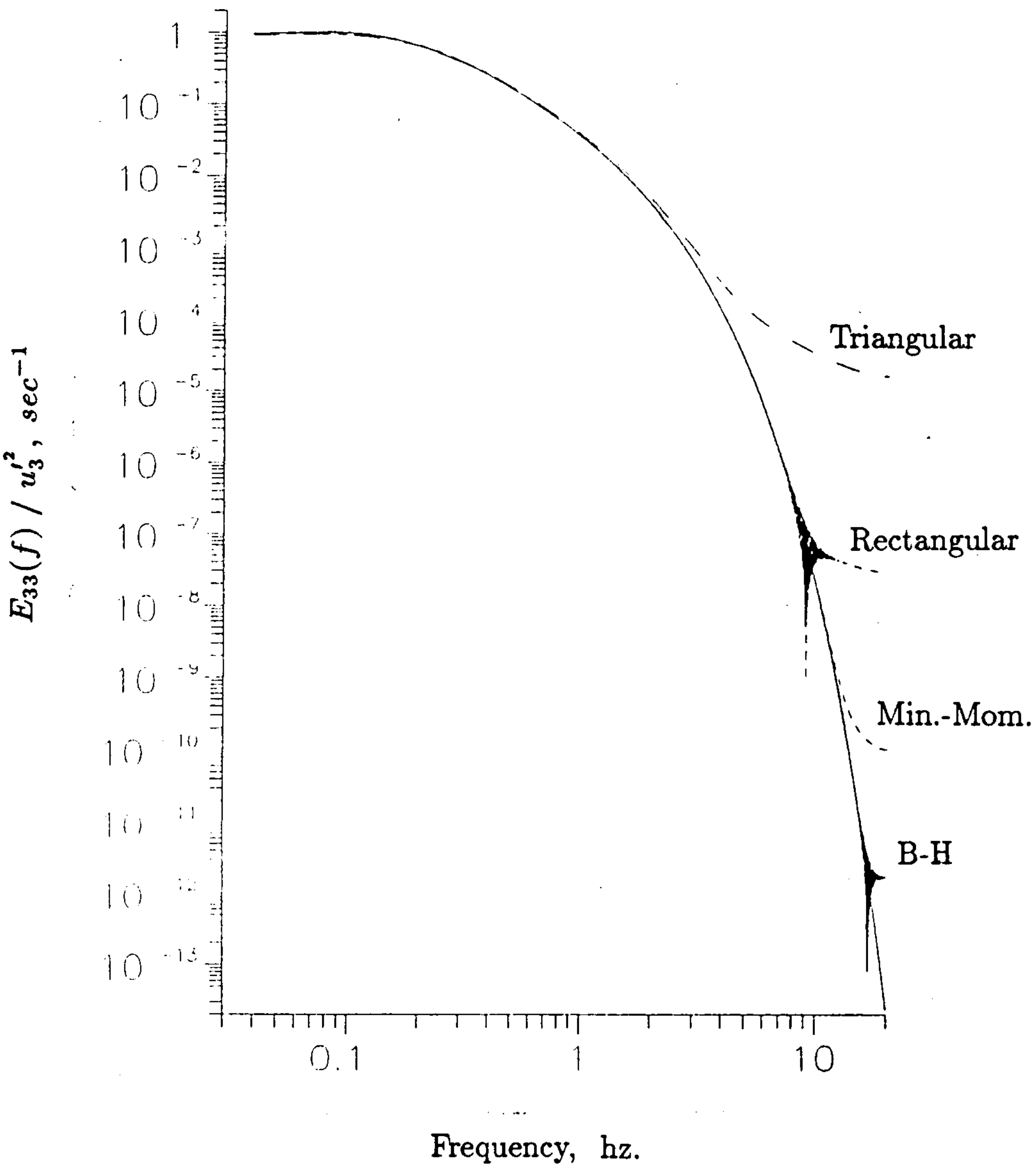

Figure 28. Effects of Windowing on the von Karman Spectrum in Direction (3,3) ($L/V = 4.0$; $s/L = 0.2$; $L_{FFT} = 512$).

CHAPTER IV

CONCLUSIONS

The following conclusions have been reached as a result of this investigation.

1. A closed form solution for both the Dryden and von Karman two-point spatial spectra have been developed and will provide meaningful models for use in design analysis of aeronautical systems.
2. For analysis where computational requirements are a significant limiting factor, the Dryden model which computes 3.5 times faster than the von Karman model may be used. Although graphically the two spectra appear to merge at high values of s/L, they differ appreciably at high and low frequencies. This difference, as a percent of the von Karman value, decreases monatomically with s/L for any given frequency. Therefore, it is not recommended that the two models be interchanged indiscriminately.
3. In the DFT computation of the one-point spatial spectra, aliasing is the primary error source. Aliasing can be minimized by sampling the data at a rate of twice the frequency for which information must be resolved. Also, filtering frequencies higher than Nyquist frequencies will also minimize aliasing error.
4. Bias error caused by truncating data records is the most significant source of error in computing two-point spatial spectra with DFT techniques. Bias errors can be minimized, but never eliminated, by windowing data records prior to processing with a DFT. The side-lobe structure of a window is the primary parameter to be considered in reducing bias error in two-point spectra analyses. The Blackman-Harris four-term window provides excellent correction of bias errors. On the other hand, the triangle or Bartlett window produces very high bias errors and should not be used for two-point spectra analysis.

REFERENCES

Abramowitz, M. and Stegun, I.A. (1964): Handbook of Mathematical Functions. Washington, D.C.: National Bureau of Standards-Applied Mathematics Series No. 55.

Diederich, F. W., and J. A. Drischler (1957): "Effect of Spanwise Variation in Gust Intensity on the Lift Due to Atmospheric Turbulence," NACA TN 3920.

Dryden, H. L. (1943): "A Review of the Statistical Theory of Turbulence," Quarterly of Applied Mathematics 1, 7-42.

Erdelyi, A. (1955):Higher Transcendental Functions. New York: McGraw-Hill.

Frost, W. (1983): "Spanwise Turbulence Modeling," Paper presented at the Ninth Conference on Aerospace and Aeronautical Meteorology of the AMS, Omaha, Neb., June 6-9.

Frost, W., amd M. C. Lin (1983): "Statistical Analysis of Turbulence Data from the NASA Marshall Space Flight Center Atmospheric Boundary Layer Tower Array Facility," NASA CR 3737.

Frost, W., H. P. Chang, and E. A. Ringnes (1987): "Analyses and Assessments of Spanwise Gust Gradient Dat from NASA B-57B Aircraft," Final report for NASA Langely Research Center under Contract NAS1-17989.

Harris, Fredric J. (1978): "On the Use of Windows for Harmonic Analysis with the Discrete Fourier Transform," Proceedings of the IEEE, Vol. 66, No. 1, 51-83.

Hinze, J. O. (1975): Turbulence. New York: McGraw-Hill.

Houbolt, J. C., and A. Sen (1972): "Cross-Spectral Functions Based on von Karman's Spectral Equation," NASA CR 2011.

Houbolt, J. C., (1973): "Atmospheric Turbulence," AIAA Journal, 4:421-437.

Kader, B. A., Yaglom, A. M., and Zubkouskii, S. L. (1989): "Spatial Correlation Functions of Surface-Layer Atmospheric Turbulence in Neutral Stratification," Boundary-Layer Meteorology 47, 233-249.

Lebedev, N. N. (1972): Special Functions and Their Applications. New York: Dover Publications.

Oppenheim, A. V. and Schafer, R. W. (1975): Digital Signal Processing. Englewood Cliffs, New Jersey: Prentice-Hall.

Papoulis, A. (1977): Signal Analysis. New York: McGraw-Hill Book Co.

Ringnes, E. A., and W. Frost (1985): "Analysis of Aerodynamic Coefficients Using Gust Gradient Data: Spanwise Turbulence Effects on Airplane Response," NASA CR 3961.

Taylor, G. I. (1938): "The Spectrum of Turbulence," Proceedings of the Royal Society, A164, 476-490.

Von Karman, T. (1948): "Progress in the Statistical Theory of Turbulence," Journal of Marine Research 7, 252-264.

APPENDIX A

DERIVATION OF THE von KARMAN TWO-POINT SPECTRA

In 1948 von Karman assumed that the turbulence spectra behaves as $(\kappa/\kappa_o)^4$ for small values of κ and is proportional to $(\kappa/\kappa_o)^{-5/3}$ for large values of κ. The parameter κ is the wave number of the fluctuation and κ_o is proportional to $1/L$, where L is a length characterizing the scale of turbulence. Based on these assumptions, von Karman proposed that the lateral correlation, $g(r)$, and the longitudinal correlation, $f(r)$, be written as follows

$$f(r) = \frac{2^{2/3}}{\Gamma(1/3)} \left(\frac{r}{L}\right)^{1/3} K_{1/3} \left(\frac{r}{L}\right) \tag{A1}$$

and

$$g(r) = \frac{2^{2/3}}{\Gamma(1/3)} \left(\frac{r}{L}\right)^{1/3} \left[K_{1/3} \left(\frac{r}{L}\right) - \frac{r}{2L} K_{2/3} \left(\frac{r}{L}\right)\right] \tag{A2}$$

Later work resulted in the term $\left(\frac{r}{L}\right)$ being modified by the term $1/a$ where

$$a = \sqrt{\pi}\, \Gamma(1/3) \,/\, \Gamma(5/6) = 1.339 \tag{A3}$$

such that defining

$$\ell = \frac{r}{1.339\, L} \tag{A4}$$

and substituting into Equations A1 and A2 yields

$$f(\ell) = \frac{2^{2/3}}{\Gamma(1/3)} (\ell)^{1/3} K_{1/3} (\ell) \tag{A5}$$

and

$$g(\ell) = \frac{2^{2/3}}{\Gamma(1/3)} \left[(\ell)^{1/3} K_{1/3}(\ell) - \frac{1}{2}(\ell)^{4/3} K_{2/3}(\ell)\right] \tag{A6}$$

For the specific case of an aircraft flying in a plane at a constant velocity (Refer to Figure 4), r in Equation A4 is replaced with $r = \sqrt{s^2 + V^2t^2}$. Equation A4 can then be written as

$$\ell = \frac{\sqrt{s^2 + V^2t^2}}{1.339L} = \frac{r}{aL} \tag{A7}$$

In Chapter II, the velocity correlation for component 1 is given by

$$Q_{11}(t) = u_1'^2 \left[\frac{f(r) - g(r)}{r^2}\,(Vt)^2 + g(r)\right]$$

where a slight change of nomenclature has been used for convenience of the derivation. That is, the subscript A, B has been dropped and should be understood in the remainder of the derivation. Also it should be understood that r is a function of time.

Introducing the notation

$$H_1 = \frac{u_1'^2\, 2^{2/3}}{\Gamma(1/3)} \tag{A8}$$

and the definitions of $f(r)$ and $g(r)$ given in Equations A5 and A6 gives

$$\begin{aligned} Q_{11}(t) =& H_1 \left[\left(\frac{Vt}{r}\right)^2 \left[\ell^{1/3}\, K_{1/3}(\ell) - \ell^{1/3}\, K_{1/3}(\ell) + \frac{\ell^{4/3}}{2}\, K_{2/3}(\ell)\right]\right. \\ & \left. + \left[\ell^{1/3}\, K_{1/3}(\ell) - \frac{\ell^{4/3}}{2}\, K_{2/3}(\ell)\right]\right] \end{aligned} \tag{A9}$$

Recall from Chapter II, Equation 11 that

$$\left(\frac{Vt}{r}\right)^2 + \left(\frac{s}{r}\right)^2 = 1 \tag{A10}$$

Solving for the term (V^2t^2/r^2) from Equation A10 and substituting into Equation A9 yields after some algebra

$$Q_{11}(l) = H_1 \left[\ell^{1/3}\, K_{1/3}(\ell) - \left(\frac{1}{2}\right) \left(\frac{s}{aL}\right)^2 \ell^{-2/3}\, K_{2/3}\,(\ell)\right] \tag{A11}$$

The definition of the two-point spatial spectra given by Equation 13 in Chapter II is

$$E_{11}(\omega) = \int_{-\infty}^{\infty} Q_{11}(t)\, e^{-i\omega t}\, dt \qquad (A12)$$

Redefining ℓ as;

$$\ell = \left[\left(\frac{V}{aL}\right)\, \left(\left(\frac{s}{V}\right)^2 + t^2\right)^{1/2}\right]$$

and substituting Equation A11 into A12 yields

$$\begin{aligned} E_{11}(w) = H_1 \int_{-\infty}^{\infty} &\left[\left(\frac{V}{aL}\right)\left(\left(\frac{s}{V}\right)^2 + t^2\right)^{1/2}\right]^{1/3} \\ &K_{1/3}\left[\left(\frac{V}{aL}\right)\left(\left(\frac{s}{V}\right)^2 + t^2\right)^{1/2}\right] e^{-i\omega t}\, dt \\ &- H_1 \left(\frac{1}{2}\right)\, \left(\frac{s}{aL}\right)^2 \int_{-\infty}^{\infty} \left[\left(\frac{V}{aL}\right)\left(\left(\frac{s}{V}\right)^2 + t^2\right)^{1/2}\right]^{-2/3} \\ &K_{2/3}\left[\left(\frac{V}{aL}\right)\left(\left(\frac{s}{V}\right)^2 + t^2\right)^{1/2}\right] e^{-i\omega t}\, dt \end{aligned} \qquad (A13)$$

Equation A13 is an even function of t. Noting that Fourier transforms of even functions can be written as two times the Fourier cosine transforms from 0 to ∞ and making use of the Bessel function relationship that $K_p(z) = K_{-p}(z)$, Equation A13 can be written as the sum of two term:

$$T1 = \int_0^{\infty} \left[\left(\frac{s}{V}\right)^2 + t^2\right]^{1/6} K_{1/3}\left[\left(\frac{V}{aL}\right)\, \left(\left(\frac{s}{V}\right)^2 + t^2\right)^{1/2}\right] cos(\omega t)\, dt \qquad (A14)$$

and

$$T2 = \int_0^{\infty} \left[\left(\frac{s}{V}\right)^2 + t^2\right]^{-1/3} K_{-2/3}\left[\left(\frac{V}{aL}\right)\, \left(\left(\frac{s}{V}\right)^2 + t^2\right)^{1/2}\right] cos(\omega t)\, dt \qquad (A15)$$

therefore

$$E_{11}(\omega) = 2H_1 \left(\frac{V}{aL}\right)^{1/3} (T1) - H_1 \left(\frac{s}{aL}\right)^2 \left(\frac{V}{aL}\right)^{-2/3} (T2) \qquad (A16)$$

Using the Fourier cosine transforms published as part of the Bateman manuscript project in Erdelyi (1955) (No. 45, Page 56) with $p = 1/3$, the solution of term $T1$ in Equation A14 becomes

$$T1 = \left(\frac{V}{aL}\right)^{1/3} \left(\frac{\pi}{2}\right)^{1/2} \left(\frac{s}{V}\right)^{5/3}$$
$$K_{-5/6}\left[\left(\frac{s}{V}\right) \left(\omega^2 + \left(\frac{s}{aL}\right)^2\right)^{1/2}\right] \left[\left(\frac{s}{V}\right) \left(\omega^2 + \left(\frac{V}{aL}\right)^2\right)^{1/2}\right]^{-5/6} \quad (A17)$$

and with $p = -2/3$, Equation A15 becomes

$$T2 = \left(\frac{\pi}{2}\right)^{1/2} \left(\frac{V}{aL}\right)^{-2/3} \left(\frac{s}{V}\right)^{-1/3}$$
$$K_{1/6}\left[\left(\frac{s}{V}\right) \left(\omega^2 + \left(\frac{V}{aL}\right)^2\right)^{1/2}\right] \left[\left(\frac{s}{V}\right) \left(\omega^2 + \left(\frac{V}{aL}\right)^2\right)^{1/2}\right]^{1/6} \quad (A18)$$

Defining z as:

$$z = \left(\frac{s}{V}\right) \left(\omega^2 + \left(\frac{V}{aL}\right)^2\right)^{1/2} \quad (A19)$$

and substituting Equations A17, A18 and A7 into Equation A16 yields

$$E_{11}(\omega) = \frac{u_1'^2 \; 2^{2/3} \; (2\pi)^{1/2} \; s^{5/3}}{\Gamma(1/3) \; V(aL)^{2/3}} \left[K_{-5/6}[z] \left(z^{-5/6}\right) - \left(\frac{1}{2}\right) K_{1/6}[z] \left(z^{1/6}\right)\right] \quad (A20)$$

Considering the second velocity correlation term given in Equation 12 of Chapter II

$$Q_{22}(t) = u_2'^2 \left[\frac{f(r) - g(r)}{r^2} \; (s)^2 + g(r)\right] \quad (A21)$$

and introducing the term H_2;

$$H_2 = \frac{u_2'^2 \; 2^{2/3}}{\Gamma(1/3)} \quad (A22)$$

along with A5 and A6, Equation A21 becomes

$$Q_{22}(l) = H_2 \left[\left(\frac{s}{aL}\right)^2 \frac{\ell^{-2/3}}{2} K_{2/3}(\ell) + \ell^{1/3} \; K_{1/3}(\ell) - \left(\frac{1}{2}\right) \ell^{4/3} \; K_{2/3}(\ell)\right] \quad (A23)$$

At this point it is necessary to introduce the recursive relationship for modified Bessel functions of the second kind, K_p, given by Lebedev (1972)

$$K_{p-1}(z) - K_{p+1}(z) = -\frac{2p}{z}\, K_p(z) \tag{A24}$$

Setting $p = 1/3$ and noting $K_{-p}(z) = K_p(z)$, Equation A24 becomes

$$K_{2/3}(z) = K_{4/3}(z) - \frac{2}{3z}\, K_{1/3}(z) \tag{A25}$$

Using this recurrence relationship A23 becomes

$$Q_{22}(l) = H_2\left[\left(\frac{4}{3}\right)\, \ell^{1/3}\, K_{1/3}(\ell) + \left(\frac{1}{2}\right)\, \left(\frac{s}{aL}\right)^2\, \ell^{-2/3}\, K_{-2/3}(\ell) - \left(\frac{1}{2}\right)\, \ell^{4/3}\, K_{4/3}(\ell)\right] \tag{A26}$$

Following the procedure used in deriving Equation A20 the two-point spatial spectrum for component 2 can be written as

$$E_{22}(\omega) = \left(\frac{8}{3}\right)\, H_2\left(\frac{V}{aL}\right)^{1/3} (T1) + H_2\left(\frac{s}{aL}\right)^2\, \left(\frac{V}{aL}\right)^{-2/3} (T2) - H_2\left(\frac{V}{aL}\right)^{4/3} (T3) \tag{A27}$$

where $T1$ and $T2$ are given by Equations A14 and A15, respectively and $T3$ is

$$T3 = \int_0^\infty \left[\left(\frac{s}{V}\right) + t^2\right]^{2/3} K_{4/3}\left[\left(\frac{V}{aL}\right)\left(\left(\frac{s}{V}\right)^2 + t^2\right)^{1/2}\right] cos(\omega t)\, dt \tag{A28}$$

Again using the Fourier cosine transform from Erdelyi (1955) with $p = 4/3$, $T3$ becomes

$$T3 = \left(\frac{\pi}{2}\right)^{1/2} \left(\frac{V}{aL}\right)^{4/3} \left(\frac{s}{V}\right)^{11/3}$$
$$K_{-11/6}\left[\left(\frac{s}{V}\right)\left(\omega^2 + \left(\frac{s}{aL}\right)^2\right)^{1/2}\right]\left[\left(\frac{s}{V}\right)\left(\omega^2 + \left(\frac{V}{aL}\right)^2\right)^{1/2}\right]^{-11/6} \tag{A29}$$

Introducing $T1, T2$ and $T3$, and the definition of z from Equation A19, the spectrum $E_{22}(\omega)$ becomes

$$E_{22}(\omega) = \frac{u_2'^2\ 2^{2/3}(2\pi)^{1/2}\ s^{5/3}}{\Gamma(1/3)\ V(aL)^{2/3}} \left[\left(\frac{4}{3}\right)\ K_{-5/6}[z]\left(z^{-5/6}\right) + \left(\frac{1}{2}\right)\ K_{1/6}[z]\left(z^{1/6}\right)\right.$$
$$\left. - \left(\frac{1}{2}\right)\left(\frac{s}{aL}\right)^2\ K_{-11/6}[z]\left(z^{-11/6}\right)\right] \tag{A30}$$

The third and last velocity correlation term given in Equation 12 of Chapter II is

$$Q_{33}(t) = u_3'^2\left[g(r)\right] \tag{A31}$$

Introducing H_3 as

$$H_3 = \frac{u_3'^2\ 2^{2/3}}{\Gamma(1/3)} \tag{A32}$$

and substituting von Karman's correlation given by Equation A6 yields

$$Q_{33}(l) = H_3\left[(\ell)^{1/3}\ K_{1/3}(\ell) - \left(\frac{1}{2}\right)\ (\ell)^{4/3}\ K_{2/3}(\ell)\right]$$

Using the recurrence relationship given by Equation A22 gives

$$Q_{33}(l) = H_3\left[\frac{4}{3}\ \ell^{1/3}\ K_{1/3}(\ell) - \left(\frac{1}{2}\right)\ \ell^{4/3}\ K_{4/3}(\ell)\right] \tag{A33}$$

Again follow the same procedure as before, the two-point spatial spectrum for Equation A33 is

$$E_{33}(\omega) = \left(\frac{8}{3}\right)\ H_3\left(\frac{V}{aL}\right)^{1/3}\ (T1) - \left(\frac{V}{aL}\right)^{4/3}\ H_3(T3) \tag{A34}$$

where the Fourier transform, $T1$ and $T3$, are given by Equations A17 and A29, respectively. Thus Equation A34 becomes

$$E_{33}(\omega) = \frac{u_3'^2\ 2^{2/3}\sqrt{2\pi}\ s^{5/3}}{\Gamma(1/3)\ (aL)^{2/3}\ V}\left[\left(\frac{4}{3}\right)\ K_{-5/6}[z]\,(z)^{-5/6} - \left(\frac{1}{2}\right)\left(\frac{s}{aL}\right)^2\ K_{-11/6}[z]\left(z^{-11/6}\right)\right] \tag{A35}$$

It is convenient for computational purposes to rewrite Equations A20, A27, and A35 in terms of

$$z = \left(\frac{s}{L}\right)\left[\left(\frac{\omega L}{V}\right)^2 + \left(\frac{1}{1.339}\right)^2\right]^{1/2}$$

$$\sigma = \frac{s}{L}$$

and

$$\nu = \frac{\omega L}{V}$$

Noting that

$$E_{ii}(\nu) = \left(\frac{V}{L}\right)\ E_{ii}(\omega)$$

then these equations become

$$E_{11}(\nu) = Cu_1'^2\ \sigma^{5/3}\left[K_{-5/6}[z]\cdot(z)^{-5/6} - \left(\frac{1}{2}\right)\ K_{1/6}[z]\left(z^{1/6}\right)\right] \qquad (A36)$$

$$E_{22}(\nu) = Cu_2'^2\ \sigma^{5/3}\left[\left(\frac{4}{3}\right)\ K_{-5/6}[z]\cdot z^{-5/6}\right.$$
$$\left. + \left(\frac{1}{2}\right)\ K_{1/6}[z]\left(z^{1/6}\right) - \left(\frac{1}{2}\right)\left(\frac{\sigma^2}{(1.339)^2}\right)\ K_{-11/6}[z]\left(z^{-11/6}\right)\right] \qquad (A37)$$

$$E_{33}(\nu) = Cu_3'^2\ \sigma^{5/3}\left[\left(\frac{4}{3}\right)\ K_{-5/6}[z]\cdot z^{-5/6}\right.$$
$$\left. - \left(\frac{1}{2}\right)\left(\frac{\sigma^2}{(1.339)^2}\right)\ K_{-11/6}[z]\left(z^{-11/6}\right)\right] \qquad (A38)$$

where

$$z = \sigma\left[(\nu)^2 + \left(\frac{1}{1.339}\right)^2\right]^{1/2}$$

$$\sigma = s/L$$

and

$$C = \left(\frac{2}{a}\right)^{2/3}\ \frac{(2\pi)^{1/2}}{\Gamma(1/3)}$$

APPENDIX B

DERIVATION OF THE DRYDEN TWO-POINT SPECTRA

In 1943 Hugh L. Dryden published (Dryden (1943)) his statistical theory of turbulence. In this analysis Dryden noted that two-point turbulence correlations curves are of the exponential type and stated that the longitudinal and lateral correlations, $f(r)$ and $g(r)$ respectively, are even functions of r/L where r is the separation distance of two points and L is a length scale which characterizes the turbulence. Dryden proposed a two-point correlations model for $f(r)$ and $g(r)$ given by

$$f(r) = e^{-r/L} \tag{B1}$$

$$g(r) = \left(1 - \frac{r}{2L}\right)\, e^{-r/L} \tag{B2}$$

For the specific case of an aircraft flying in a plane with a constant velocity (refer to Figure 4 in Chapter II), the term r in Equations B1 and B2 must be replaced with the term $r = \sqrt{s^2 + (Vt)^2}$. Also in Chapter II, the first velocity correlation term in Equation 12 was

$$Q_{11}(t) = u_1'^2 \left[\frac{f(r) - g(r)}{r^2} (Vt)^2 + g(r) \right]$$

Replacing r with $\sqrt{s^2 + (Vt)^2}$ in Equation B1 and B2, this Equation becomes

$$\begin{aligned} Q_{11}(t) &= u_1'^2 \left[\left[e^{-r/L} - (1 - \frac{r}{2L}\, e^{-r/L} \right] \left(\frac{Vt}{r}\right)^2 + \left[\left(1 - \frac{r}{2L}\right)\, e^{-r/L} \right] \right] \\ &= u_1'^2 \left[\left(\frac{r}{2L}\right) \left(\frac{Vt}{r}\right)^2 e^{-r/L} + e^{-r/L} - \left(\frac{r}{2L}\right)\, e^{-r/L} \right] \end{aligned} \tag{B3}$$

But from Chapter II, Equation 11

$$\left(\frac{Vt}{r}\right)^2 + \left(\frac{s}{r}\right)^2 = 1 \tag{B4}$$

Solving for the term $(Vt/r)^2$ in Equation B4 and substituting into Equation B3 yields

$$Q_{11}(t) = u_1'^2 \left[e^{-s/L} - \left(\frac{r^2}{2Ls}\right)\ e^{-s/L}\right] \tag{B5}$$

The second velocity correlation term given in Equation 12 of Chapter II was

$$Q_{22}(t) = u_2'^2 \left[\frac{f(r) - g(r)}{r^2}\ (s)^2 + g(r)\right]$$

In terms of the Dryden correlation model with $r = \sqrt{s^2 + (Vt)^2}$ this becomes

$$Q_{22}(t) = u_2'^2 \left[\left(\frac{s^2}{2rL}\right)\ e^{-r/L} + e^{-r/L} - \left(\frac{r}{2L}\right)\ e^{-r/L}\right] \tag{B6}$$

The third velocity correlation term given in Equation 12 of Chapter II was

$$Q_{33}(t) = u_3'^2\ [g(r)]$$

Which for the Dryden model can be written as

$$Q_{33}(t) = u_3'^2 \left[e^{-r/L} - \left(\frac{r}{2L}\right)\ e^{-r/L}\right] \tag{B7}$$

Rewriting the term r as

$$r = V\left[\left(\frac{s}{V}\right)^2 + t^2\right]^{\frac{1}{2}}$$

And substituting into Equations B5, B6, and B7 yields

$$Q_{11}(t) = u_1'^2 \left[e^{-(\frac{V}{L})\left[(\frac{s}{V})^2+t^2\right]^{\frac{1}{2}}} - \left(\frac{s^2}{2VL}\right)\ \frac{e^{-(\frac{V}{L})[(\frac{s}{V})^2+t^2]^{\frac{1}{2}}}}{[(\frac{s}{V})^2 + t^2]^{\frac{1}{2}}}\right] \tag{B8}$$

$$Q_{22}(t) = u_2'^2 \left[e^{-(\frac{V}{L})[(\frac{s}{V})^2+t^2]^{\frac{1}{2}}} + \left(\frac{s^2}{2VL}\right) \frac{e^{-(\frac{V}{L})[(\frac{s}{V})^2+t^2]^{\frac{1}{2}}}}{[(\frac{s}{V})^2+t^2]^{\frac{1}{2}}} - \left(\frac{V}{2L}\right) \frac{e^{-(\frac{V}{L})[(\frac{s}{V})^2+t^2]^{\frac{1}{2}}}}{[(\frac{s}{V})^2+t^2]^{-\frac{1}{2}}} \right] \quad (B9)$$

$$Q_{33}(t) = u_3'^2 \left[e^{-(\frac{V}{L})[(\frac{s}{V})^2+t^2]^{\frac{1}{2}}} - \left(\frac{V}{2L}\right) \frac{e^{-(\frac{V}{L})[(\frac{s}{V})^2+t^2]^{\frac{1}{2}}}}{[(\frac{s}{V})^2+t^2]^{-\frac{1}{2}}} \right] \quad (B10)$$

The definition of the two-point spatial spectra is

$$E_{ii}(\omega) = \int_{-\infty}^{\infty} Q_{ii}(t)\, e^{-j\omega t}\, dt \quad (B11)$$

which is the Fourier transform of the velocity correlation. This requires that each of the Equations B8, B9, and B10 be transformed. From inspection, it can be seen that Equations B8, B9 and B10 contain only three complicated forms of the exponential. The Fourier transform of Equations B8, B9, and B10 can be accomplished by taking the Fourier transform of these three exponential terms, multiplying them by the appropriate constants, and then sum the resulting terms as defined by Equations B8, B9, and B10. The three transforms are defined as follows

$$T1 = \int_{-\infty}^{\infty} e^{-(\frac{V}{L})[(\frac{s}{V})^2+t^2]^{\frac{1}{2}}}\, e^{-i\omega t}\, dt \quad (B12)$$

$$T2 = \int_{-\infty}^{\infty} \left[\left(\frac{s}{V}\right)^2 + t^2\right]^{\frac{1}{2}} e^{-(\frac{V}{L})[(\frac{s}{V})^2+t^2]^{\frac{1}{2}}}\, e^{-i\omega t}\, dt \quad (B13)$$

$$T3 = \int_{-\infty}^{\infty} \left[\left(\frac{s}{V}\right)^2 + t^2\right]^{-\frac{1}{2}} e^{-(\frac{V}{L})[(\frac{s}{V})^2+t^2]^{\frac{1}{2}}}\, e^{-i\omega t dt} \quad (B14)$$

Equations B12, B13, and B14 are all even functions of t since only squared terms of t appear in the equations, then the exponential Fourier transform can be written as two times the Fourier cosine transform such that

$$T1 = 2\int_{0}^{\infty} e^{-(\frac{V}{L})[(\frac{s}{V})^2+t^2]^{\frac{1}{2}}}\, cos(\omega t)\, dt \quad (B15)$$

$$T2 = 2\int_0^{\infty}\left[\left(\frac{s}{V}\right)^2 + t^2\right]^{\frac{1}{2}} e^{-(\frac{V}{L})[(\frac{s}{V})^2+t^2]^{\frac{1}{2}}} \; cos(\omega t)\; dt \qquad (B16)$$

$$T3 = 2\int_0^{\infty}\left[\left(\frac{s}{V}\right)^2 + t^2\right]^{-\frac{1}{2}} e^{-(\frac{V}{L})[(\frac{s}{V})^2+t^2]^{\frac{1}{2}}} \; cos(\omega t)\; dt \qquad (B17)$$

A review of all available Fourier transforms revealed that while transforms for Equations B15 and B17 are readily available there is no published transform for Equation B16. In order to develop a closed form solution for the spectra from Dryden's correlation model, a Fourier transform for Equation B16 was derived. Since the key to an analytical solution is solving Equation B16, it will be carried out first.

The approach taken to solve Equation B16 is to integrate it by parts, such that the following relationship holds

$$\int u dv = uv - \int v du \qquad (B18)$$

The key to this approach is separating Equation B16 into parts in such a way as to have a new integral for which a transform is tabulated. Integrating by parts where

$$u = \left[\left(\frac{s}{V}\right)^2 + t^2\right]^{\frac{1}{2}} e^{-(\frac{V}{L})[(\frac{s}{V})^2+t^2]^{\frac{1}{2}}}$$

and

$$dv = cos(\omega t)\; dt$$

allows Equation B16 to be rewritten as

$$\begin{aligned} T2 =& \frac{2}{\omega}\left[\left[\left(\frac{s}{V}\right)^2 + t^2\right]^{\frac{1}{2}} e^{-(\frac{V}{L})[(\frac{s}{V})^2+t^2]^{\frac{1}{2}}} \; sin(\omega t)\right]\Bigg|_0^{\infty} \\ & - \frac{2}{\omega}\int_0^{\infty} \frac{t\; e^{-(\frac{V}{L})[(\frac{s}{V})^2+t^2]^{\frac{1}{2}}}}{[(\frac{s}{V})^2+t^2]^{\frac{1}{2}}}\; sin(\omega t)\; dt \qquad (B19) \\ & + \frac{2V}{\omega L}\int_0^{\infty} t\; e^{-(\frac{V}{L})[(\frac{s}{V})^2+t^2]^{\frac{1}{2}}} \; sin(\omega t)\; dt \end{aligned}$$

The first term on the right hand side of Equation B19 is evaluated at 0 and ∞. This term is zero at zero since the sine of zero is equal to zero. At ∞ it is undefined. However the function is of exponential order and will go to zero as $t \rightarrow -\infty$. Therefore, the first term in Equation B19 is zero.

For the other two terms in Equation B19, the Fourier sine transforms published as part of the Bateman manuscript project in Erdelyi (1955) applies. From Equation B19, Term 2 is defined as

$$\text{Term 2} = -\frac{2}{\omega}\int_0^\infty \frac{t\ e^{-(\frac{V}{L})[(\frac{s}{V})^2+t^2]^{\frac{1}{2}}}}{[(\frac{s}{V})^2+t^2]^{\frac{1}{2}}}\ sin(\omega t)\ dt$$

From Erdelyi (1955), Page 75, transform No. 36, this becomes

$$\text{Term 2} = \frac{-2(\frac{s}{V})^2\ K_1[(\frac{s}{V})((\frac{V}{L})^2+\omega^2)^{\frac{1}{2}}]}{(\frac{s}{V})((\frac{V}{L})^2+\omega^2)^{\frac{1}{2}}} \tag{B21}$$

The third term in Equation B19 is given as

$$\text{Term 3} = \frac{2V}{\omega L}\int_0^\infty t\ e^{-(\frac{V}{L})[(\frac{s}{V})^2+t^2]^{\frac{1}{2}}}\ sin(\omega t)\ dt$$

Again from Erdelyi (1955), Page 75, transform No. 35, this becomes

$$\text{Term 3} = 2\ \frac{(\frac{V}{L})^2(\frac{s}{V})\ K_2[(\frac{s}{V})((\frac{V}{L})^2+\omega^2)^{\frac{1}{2}}]}{[(\frac{s}{V})((\frac{V}{L})^2+\omega^2)^{\frac{1}{2}}]^2}$$

The solution of Equation B19 can now be written as the sum of Term 1, Term 2, and Term 3 as follows. First, however, introducing the term

$$z = \left(\frac{s}{V}\right)\left(\left(\frac{V}{L}\right)^2+\omega^2\right)^{\frac{1}{2}} \tag{B22}$$

Then

$$T2 = 0 - 2\left(\frac{s}{V}\right)^2 K_1(z)(z)^{-1} + 2\left(\frac{s}{V}\right)^4 \left(\frac{V}{L}\right)^2 K_2(z)(z)^{-2} \qquad (B23)$$

Again considering Equation B15, the Fourier cosine transform given in Erdelyi (1955), Page 16, No. 26 allows for T1 to be written as

$$T1 = 2\left[\left(\frac{s}{V}\right)\left(\frac{V}{L}\right)\left[\left(\frac{V}{L}\right)^2 + \omega^2\right]^{-\frac{1}{2}} K_1\left[\left(\frac{s}{V}\right)\left(\left(\frac{V}{L}\right)^2 + \omega^2\right)^{\frac{1}{2}}\right]\right]$$

Upon substitution of z from Equation B22, becomes

$$T1 = 2\left(\frac{V}{L}\right)\left(\frac{s}{V}\right)^2 K_1(z)\,[z]^{-1} \qquad (B24)$$

The Fourier cosine transform of Equation B17 is, from Erdelyi (1955), Page 17, No. 27,

$$T3 = 2 \cdot K_0\left[\left(\frac{s}{V}\right)\left(\left(\frac{V}{L}\right)^2 + \omega^2\right)^{\frac{1}{2}}\right]$$

Again using the definition for z, this becomes

$$T3 = 2K_0\,[z] \qquad (B25)$$

The two-point spatial spectra for the Dryden correlation model can be written using Equations B23, B24, and B25. The general spatial spectra given by Equation B11 when applied to the correlation given by Equation B8 yields

$$\begin{aligned} E_{11}(\omega) &= u_1'^2\left[\frac{2(\frac{V}{L})(\frac{s}{V})^2\,K_1[z]}{(z)} - \left(\frac{s^2}{LV}\right)K_0[z]\right] \\ &= u_1'^2\left[2\left(\frac{s^2}{LV}\right)\right]\left[K_1[z]\cdot(z)^{-1} - \left(\frac{1}{2}\right)K_0[z]\right] \end{aligned} \qquad (B26)$$

In a similar manner

$$E_{22}(\omega) = u_2'^2 \Bigg[2\left(\frac{V}{L}\right) \left(\frac{s}{V}\right)^2 K_1(z)(z)^{-1} + \left(\frac{s^2}{VL}\right) \left(K_0(z)\right)$$

$$- \left(\frac{V}{2L}\right) \left[2 \left(\frac{s}{V}\right)^4 \left(\frac{V}{L}\right)^2 K_2(z) \cdot (z)^{-2} - 2 \left(\frac{s}{V}\right)^2 K_1(z)(z)^{-1} \right] \Bigg]$$

$$E_{22}(\omega) = 2u_2'^2 \left(\frac{s^2}{VL}\right) \Bigg[\frac{3}{2} K_1[z\ ](z)^{-1} + \left(\frac{1}{2}\right) K_0[z]$$

$$- \left(\frac{1}{2} \cdot \frac{s^2}{L^2}\right) K_2[z] \cdot (z)^{-2} \Bigg] \tag{B27}$$

and term $E_{3,3}(\omega)$ can be written as

$$E_{33}(\omega) = 2u_3'^2 \left(\frac{s^2}{VL}\right) \left[\frac{3}{2} K_1[z](z)^{-1} - \frac{1}{2} \left(\frac{s^2}{L^2}\right) \frac{K_2[z]}{(z)^2} \right] \tag{B28}$$

Equations B26, B27, and B28 are the closed form solutions of the two-point spatial spectra based on the Dryden correlation model. For computational purposes these equations will be rewritten. First consider Equation B22 and redefining z such that

$$z = \left(\frac{s}{L}\right) \left[\left(\frac{\omega L}{V}\right)^2 + 1 \right]^{\frac{1}{2}}$$

Now introducing the terms $\sigma = s/L$, and

$$\nu = \left(\frac{\omega L}{V}\right) \tag{B29}$$

as well as, the fact that

$$E_{i,i}(\omega) = \left(\frac{V}{L}\right) E_{i,i}(\nu)$$

Equation B26 can be written as

$$E_{11}(\nu) = 2u_1'^2\ \sigma^2 \left[K_1[z](z)^{-1} - \left(\frac{1}{2}\right) K_0[z] \right] \tag{B30}$$

Equation B27 becomes

$$\begin{aligned} E_{22}(\nu) = 2u_2'^2\ \sigma^2 \ & \left[\frac{3}{2}\ K_1[z](z)^{-1} + \left(\frac{1}{2}\right)\ K_0[z] \right. \\ & \left. - \left(\frac{1}{2}\right)\ \sigma^2 K_2[z](z)^{-2} \right] \end{aligned} \tag{B31}$$

and Equation B28 becomes

$$E_{33}(\nu) = 2u_3'^2\ \sigma^2 \left[\frac{3}{2}\ K_1[z](z)^{-1} - \left(\frac{1}{2}\right)\ \sigma^2 K_2[z](z)^{-2} \right] \tag{B32}$$

VITA

Joseph E. Durham, Jr. was born in Baltimore, Maryland on January 26, 1943. His parents are Joseph E. Durham, Sr. and the former Lucy Payne Hulgan both of Dekalb County, Alabama. He graduated from Fort Payne High School, Fort Payne, Alabama in May 1961. That fall he entered the University of Alabama majoring in aerospace engineering. He graduated from the University of Alabama in 1966 with a BSAE degree.

Mr. Durham moved to Huntsville, Alabama after graduation to work for the Chrysler Corp. on the Saturn IB Space Program. He entered a graduate engineering program at the University of Alabama in Huntsville that fall. Attending only night school, he graduated in 1971 with a Master of Science in Engineering degree with a major in theoretical fluids and a minor in engineering mechanics.

In 1969, Mr. Durham joined the U.S. Army Missile and Space Intelligence Center (MSIC) as an aerospace engineer on Redstone Arsenal in Huntsville, Alabama. Mr. Durham has been with MSIC for 21 years, working in a variety of technical and managerial positions. He spent eight years developing six-degree-of-freedom digital simulations of threat missile systems to include RF seekers and advanced guidance and control concepts.

Mr. Durham has been involved in numerous special projects during his career to include developing the first U.S. surrogate of a ground-based phased array pulsed-doppler threat radar system and the development of the Airborne RF Seeker Test Bed to replicate advanced threat seekers. He was also the principal engineer and director of the Tri-service team which developed the threat design for the hardware simulator of the SA-11 missile system.

Mr. Durham is currently Chief of the CROSSBOW-S Management Office. In this capacity he serves as a senior scientific and engineering advisor and consultant to the Director of MSIC in the area of Soviet Air Defense Systems. He is also Chairman of the OSD chartered CROSSBOW-S Committee charged with the responsibility of reviewing and coordinating all aspects of the DoD development and acquisition programs for both hardware and software simulators of Soviet air defense systems used for operational testing, developmental testing and training. As Chairman of CROSSBOW-S he is a member of the DoD Joint Executive Committee on Air Defense Threat Simulators (EXCOM) and a principal technical advisor to the OSD/Deputy Director Defense, Research, and Engineering (T&E) who chairs the EXCOM.

Mr. Durham is married to the former Betty Jane Bailey of Akron, Alabama. They have two children: a daughter, Ashley Shea, 19, who is attending the University of Alabama; and a son, Joseph Tyler, 16, who is attending Grissom High School. Mr. Durham is currently a member of the Phi Kappa Phi National Honorary.